Article

Cancer Cell

Genetic and pharmacological modulation of DNA mismatch repair heterogeneous tumors promotes immune surveillance

Graphical abstract

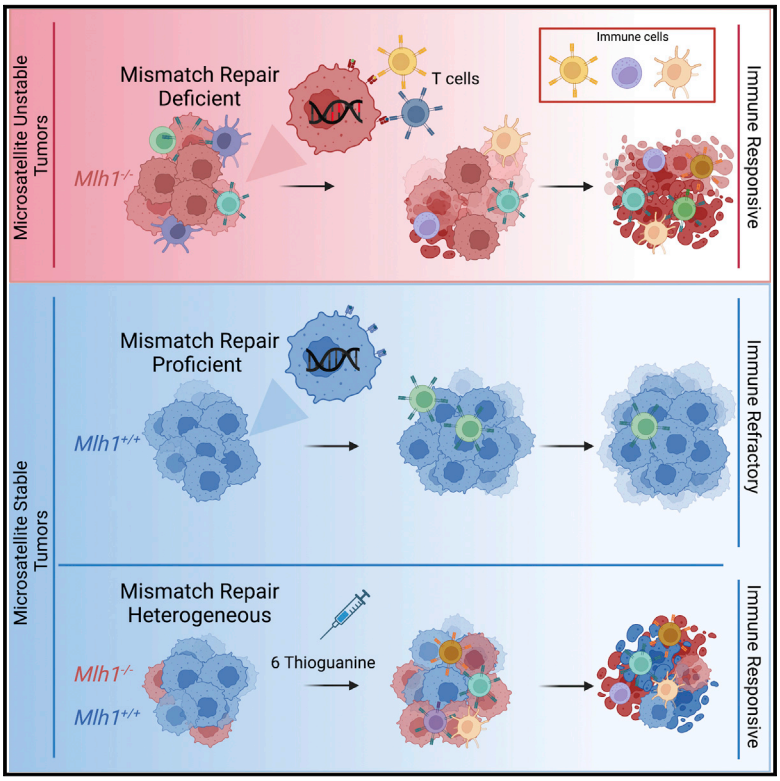

Highlights

- MMR heterogeneity affects immune surveillance in mouse CRC
- *In vivo* 6TG treatment increases the MMRd fraction of MMR heterogeneous tumors
- Pharmacological selection of MMRd cells improves immune surveillance in MMR tumors

Authors

Vito Amodio, Simona Lamba, Rosaria Chilà, ..., Federica Di Nicolantonio, Giovanni Germano, Alberto Bardelli

Correspondence

giovanni.germano@unito.it (G.G.), alberto.bardelli@unito.it (A.B.)

In brief

The impact of MMR heterogeneity on immune surveillance of colon cancers is largely unexplored. This proof-of-concept study by Amodio et al. suggests that MMR heterogeneity can be exploited through an endogenous vaccination approach based on pharmacological modulation of the DNA MMR, which potentiates cancer immunogenicity.

Amodio et al., 2023, Cancer Cell *41*, 196–209
January 9, 2023
https://doi.org/10.1016/j.ccell.2022.12.003

CellPress

CellPress
OPEN ACCESS

Cancer Cell

Article

Genetic and pharmacological modulation of DNA mismatch repair heterogeneous tumors promotes immune surveillance

Vito Amodio,[1,2,11] Simona Lamba,[2] Rosaria Chilà,[1,3] Chiara M. Cattaneo,[3] Benedetta Mussolin,[2] Giorgio Corti,[1,2] Giuseppe Rospo,[1,2] Enrico Berrino,[2,8] Claudio Tripodo,[3,7] Federica Pisati,[9] Alice Bartolini,[2] Maria Costanza Aquilano,[10] Silvia Marsoni,[3] Gianluca Mauri,[3,4] Caterina Marchiò,[2,8] Sergio Abrignani,[5,6] Federica Di Nicolantonio,[1,2] Giovanni Germano,[1,2,12,*] and Alberto Bardelli[1,2,11,12,13,*]

[1]Department of Oncology, University of Torino, 10060 Candiolo, TO, Italy
[2]Candiolo Cancer Institute, FPO - IRCCS, 10060 Candiolo, TO, Italy
[3]IFOM ETS - The AIRC Institute of Molecular Oncology, 20139 Milan, Italy
[4]Department of Oncology and Hemato-Oncology, University of Milan, 20162 Milan, Italy
[5]Istituto Nazionale Genetica Molecolare INGM 'Romeo ed Enrica Invernizzi', 20122 Milan, Italy
[6]Department of Clinical Sciences and Community Health, University of Milan, 20122 Milan, Italy
[7]Tumor Immunology Unit, Department of Health Sciences, University of Palermo, 90127 Palermo, Italy
[8]Department of Medical Sciences, University of Torino, Torino, Italy
[9]Histopathology Unit, Cogentech S.C.a.R.L., 20139, Milan, Italy
[10]Department of Hematology, Oncology, and Molecular Medicine, ASST Grande Ospedale Metropolitano Niguarda, 20162 Milan, Italy
[11]Present address: Department of Oncology, University of Torino, Italy and IFOM ETS – The AIRC Institute of Molecular Oncology, Milan, Italy
[12]These authors contributed equally
[13]Lead contact
*Correspondence: giovanni.germano@unito.it (G.G.), alberto.bardelli@unito.it (A.B.)
https://doi.org/10.1016/j.ccell.2022.12.003

SUMMARY

Patients affected by colorectal cancer (CRC) with DNA mismatch repair deficiency (MMRd), often respond to immune checkpoint blockade therapies, while those with mismatch repair-proficient (MMRp) tumors generally do not. Interestingly, a subset of MMRp CRCs contains variable fractions of MMRd cells, but it is unknown how their presence impacts immune surveillance. We asked whether modulation of the MMRd fraction in MMR heterogeneous tumors acts as an endogenous cancer vaccine by promoting immune surveillance. To test this hypothesis, we use isogenic MMRp (*Mlh1*$^{+/+}$) and MMRd (*Mlh1*$^{-/-}$) mouse CRC cells. MMRp/MMRd cells mixed at different ratios are injected in immunocompetent mice and tumor rejection is observed when at least 50% of cells are MMRd. To enrich the MMRd fraction, MMRp/MMRd tumors are treated with 6-thioguanine, which leads to tumor rejection. These results suggest that genetic and pharmacological modulation of the DNA mismatch repair machinery potentiate the immunogenicity of MMR heterogeneous tumors.

INTRODUCTION

In mammalian cells, protein complexes consisting of MutL homolog 1 (MLH1), MutS protein homolog 2 (MSH2), MutS homolog 6 (MSH6), and PMS1 homolog 2 (PMS2) execute post-replicative DNA mismatch repair (MMR).[1,2] The MMR machinery maintains DNA replication fidelity and it is required for detection and replacement of single nucleotide mismatches that escape proofreading during replication.[1,2] MMR also amends small insertions and deletions that can occur when replication complexes move across repetitive sequences, so-called microsatellites.[2] Loss of MMR proficiency is associated with microsatellite instability (MSI).[1] MMR deficiency does not directly promote cell proliferation, but tumors carrying defects in MMR repair genes accumulate a high mutational burden, a feature linked to rapid progression, but also to a favorable prognosis in colorectal cancer (CRC).[3–5]

Mismatch repair deficiency (MMRd) is observed in approximately 30% of endometrial cancers, 20% of gastric cancers, and 15% of CRCs, as well as in other tumor types at lower prevalence.[6,7] MMRd/MSI testing is recommended in all CRC cases for Lynch syndrome screening and in stage II CRC to define patients with a lower risk of recurrence and better overall survival.[8] Importantly, independent of the primary tumor histology, MMRd cancers often retain high sensitivity to immune-checkpoint blockade (ICB) therapy. Accordingly, the anti-programmed death cell protein-1 (PD-1) antibodies pembrolizumab and dostarlimab were recently approved by the U.S. Food and Drug

Administration for the treatment of any advanced MMRd solid tumor.[9–12]

Classification of tumors based on MSI status can be performed by PCR assays and/or by immunohistochemistry (IHC).[13–15] The use of IHC has been recommended as the first-line screening method to define MSI/MMRd status for prognostic and therapeutic purposes.[16] The determination of MSI status using both methods has shown some discordance that may stem from technical issues or biological reasons.[17] However, even after resolving technical issues, several studies have confirmed the presence of heterogeneity encompassing microsatellite stable (MSS) and MSI tumor components in CRC as well as gastric, pancreatic, and breast cancers.[17–21] In a subset of tumors ultimately classified as MSS, areas of weak or no MMR protein expression intermingled with regions with strong and diffuse expression have been described by multiple authors.[17,20,22–24] Notably, heterogeneity in MMR protein expression mirrors heterogeneous molecular patterns of genetic or epigenetic alterations in MMR genes.[17,20,23] Different levels of MMR protein expression heterogeneity have been reported. In 2002, Chapusot et al. described different patterns of MMR heterogeneity in 8 of 100 right-sided CRC cancer patients; among the 8 heterogeneous samples, 2 were characterized by focal loss of a single MMR protein, whereas the others displayed aberrant staining of 2 or more MMR markers.[22] Peculiar patterns/mosaicisms of a single MMR player have been reported in around 1% of CRC.[20] Variability in reported rates may stem from three factors: the limited biological material exploited to assess the MMR status, the methods used (IHC-based vs. DNA-based methods), and the existence of different patterns of MMR heterogeneity as described by Joost et al.[25]

Of relevance, it was recently reported that a patient with metastatic CRC (mCRC) displaying immunohistochemical and molecularly heterogeneous patterns of MSI in the primary tumor showed a remarkable response to ICB therapy, resulting in prolonged disease stabilization.[20] Upon IHC examination, up to 50% of the tumor tissue showed complete loss of MLH1, while other areas had marked MLH1/PMS2 positivity.[20] PCR-based MSI testing further confirmed MMR heterogeneity, while the absence of genetic alterations suggested epigenetic silencing of the *MLH1* promoter as a mechanism of MMR function impairment.[20] Upon treatment with anti PD-1 and anti-cytotoxic T lymphocyte antigen 4 antibodies, the patient achieved a major and lasting clinical benefit.[20]

Beyond pre-existing heterogeneous patterns of MMR alterations, MMR heterogeneity can be acquired as a result of therapeutic treatment. In the Pembrolizumab in MMR-Proficient Metastatic Colorectal Cancer Pharmacologically Primed to Trigger Hypermutation Status (ARETHUSA) trial, we recently demonstrated how MMR status can be pharmacologically altered through treatment with temozolomide (TMZ).[26] In this study, multiple alterations in MMR genes were detected in association with the emergence of the TMZ signature in tumors' DNA; notably, the p.T1219I MSH6 variant was detected in circulating tumor DNA and tissue of 94% (16/17) of mCRC previously classified as MSS. In the majority of patients, the acquisition of a TMZ signature, high tumor mutational burden (TMB), and alteration of MMR machinery gene expression arose in a subset of the tumors' cells, thus leading to a disease in which MSS and MSI subclones coexist. The ARETHUSA trial represents proof of concept that acquired MMR heterogeneity can also arise in a MMRp context as a consequence of treatment with an alkylating agent such as TMZ. Notably, in four of six patients, the acquisition of these MMR alterations was associated with prolonged disease stabilization upon pembrolizumab treatment.[26]

Based on this evidence, we hypothesized that the presence of immunogenic MMRd/MSI cells within a MMRp/MSS tumor could trigger immunity and this might restrict tumor growth. How and to what extent the presence of a subclonal MMRd component impacts immune surveillance in CRC patients harboring pre-existing or acquired MMR heterogeneity is largely unknown. To address the therapeutic relevance of intra-tumoral MMRd heterogeneity, we developed and analyzed mouse cancer models displaying different levels of MMRd heterogeneity.

RESULTS

The MMRd cellular fraction affects the growth of MMRd/MMRp heterogeneous tumors in immunocompetent mice

We previously used genome editing to generate colorectal, pancreatic and breast cancer cells lacking the *Mlh1* gene (*Mlh1*$^{-/-}$).[27] The derivative cells display MSI, increased tumor mutational burden and higher levels of predicted neoantigens.[27] *Mlh1*$^{-/-}$ cells grow poorly when injected in syngeneic mouse models, and when they generate tumors, these are remarkably sensitive to ICB therapy.[27] For example, murine CRC CT26 *Mlh1*$^{-/-}$ cells cultured for several months *in vitro* display high immunogenicity *in vivo* and their growth in syngeneic mice is impaired.[27] To explore the effect of intra-tumoral molecular heterogeneity on the anti-tumor immune response, we created heterogeneous cellular populations with different proportions (20/80, 80/20) of MMRp (*Mlh1*$^{+/+}$) and MMRd (*Mlh1*$^{-/-}$) CT26 isogenic cells (Figure S1A) and then injected them (5×10^5 cells) into mice. Homogeneous populations composed entirely of *Mlh1*$^{+/+}$ or *Mlh1*$^{-/-}$ cells served as controls. Droplet digital PCR (ddPCR) probes were designed to detect and accurately quantify *Mlh1*$^{+/+}$ and *Mlh1*$^{-/-}$ variants in genomic DNA (gDNA) extracted from the heterogeneous populations (Figure S1B).

Populations containing different proportions of MMRp and MMRd isogenic cells were injected in syngeneic mice and tumor development was monitored over time (Figure 1A). The growth of MMRp and MMRd heterogeneous tumors was delayed proportionally to the fraction of MMRd CRC cells they contained (Figure 1B). The presence of only 20% MMRd cells was sufficient to delay tumor growth, suggesting that the MSI fraction could have a bystander anti-tumor effect on the MSS component. Interestingly, two of six mice injected with a population comprising 80% MMRd cells did not develop a palpable tumor, suggesting that a small MSS component in an otherwise MSI tumor does not always lead to cancer growth (Figure 1C).

Next, we assessed whether MMR heterogeneous tumor growth delay was driven by a reduced engraftment of *Mlh1*$^{+/+}$ cells after the immune editing of *Mlh1*$^{-/-}$ counterpart. MMRp cells were able to form tumor that grew also when the number of injected cells was lower (Figure 1D). A growing tumor was established in the majority of mice injected with 1×10^5

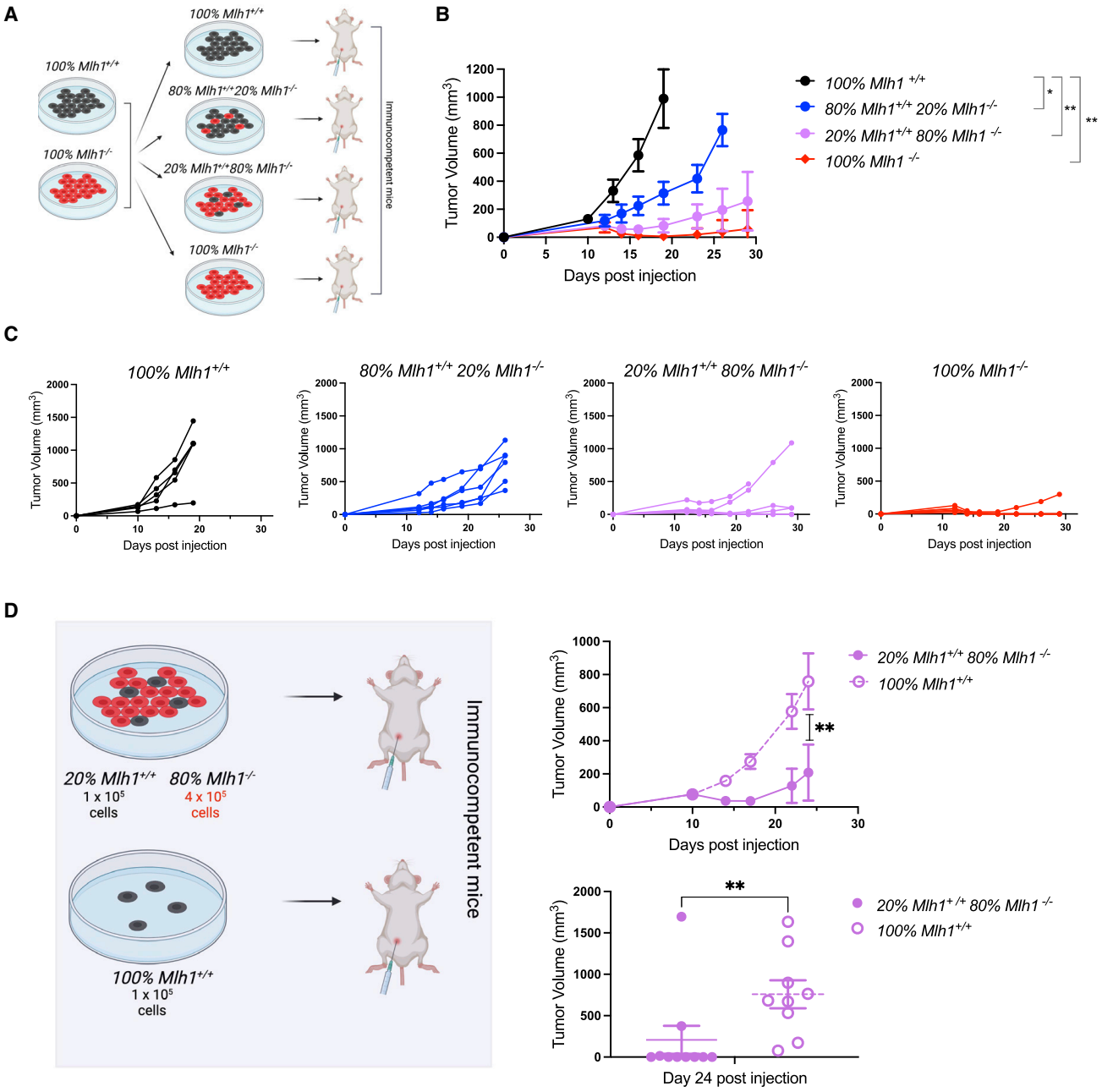

Figure 1. MMR heterogeneity affects tumor growth

(A) Heterogeneous cell populations (100% *Mlh1*$^{+/+}$, 80% *Mlh1*$^{+/+}$ 20% *Mlh1*$^{-/-}$, 20% *Mlh1*$^{+/+}$ 80% *Mlh1*$^{-/-}$, and 100% *Mlh1*$^{-/-}$) were subcutaneously injected in immunocompetent BALB C mice (5 × 10^5 cells per mouse).

(B) Tumor growth was monitored twice a week and is reported in the graph as average of tumor volumes (mm^3) ± standard error of the mean. (C) Tumor volumes (mm^3) of single mice are listed. Each experimental group was composed at least of five animals.

(D) CT26 *20%Mlh1*$^{+/+}$ 80%*Mlh1*$^{-/-}$ (1 × 10^5 *Mlh1*$^{+/+}$+ 4 × 10^5 *Mlh1*$^{-/-}$ cells) mixed population and the relative control (1 × 10^5 *Mlh1*$^{+/+}$cells alone) were injected in immunocompetent syngeneic mice. Ten mice were included in each group. Tumor growth was monitored twice a week. The average tumor volume (mm^3) ± standard error of the mean and single tumor volumes at day 24 are reported. These experiments were performed once. Mann-Whitney statistical analyses was performed: *p < 0.05; **p < 0.01. See also Figure S1A.

Mlh1$^{+/+}$ cells (corresponding with the number of *Mlh1*$^{+/+}$ cells present in the 80% *Mlh1*$^{-/-}$ 20% *Mlh1*$^{+/+}$mix). Notably, the growth of the same amount of *Mlh1*$^{+/+}$ cells in the presence of the MMRd (4 × 10^5 *Mlh1*$^{-/-}$ cells) counterpart was severely impaired, the majority of mice rejected the tumor and remained tumor free (Figure 1D). These data suggest that tumor growth delay and tumor rejection observed in *Mlh1*$^{+/+}$ *Mlh1*$^{-/-}$ mix is due to an active mechanism that impairs tumor growth, and it is not a consequence of bias due to the residual number of *Mlh1*$^{+/+}$ cells upon immunoediting of *Mlh1*$^{-/-}$cells.

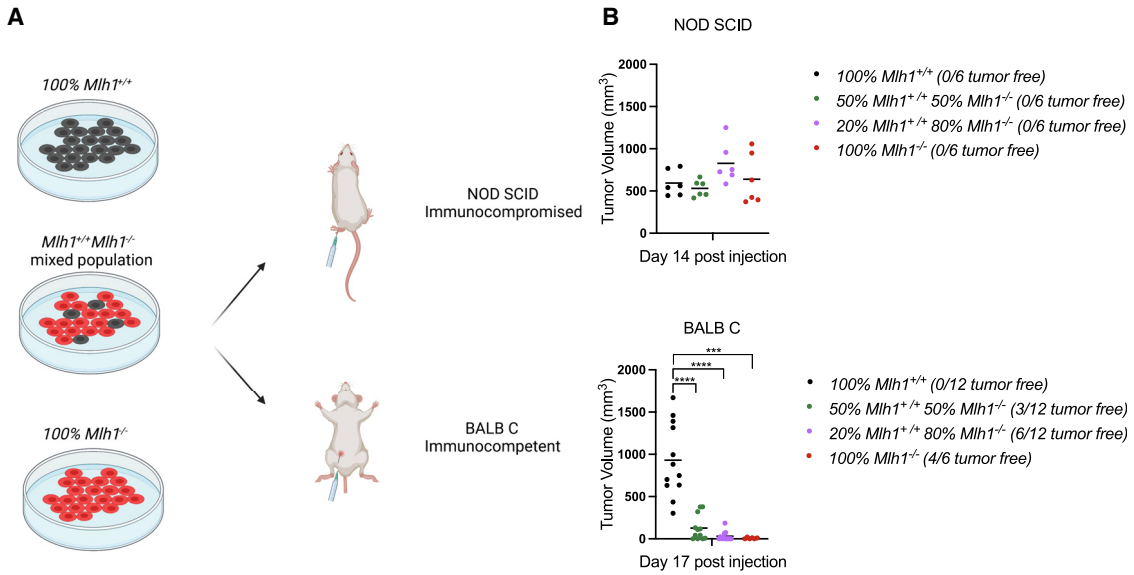

Figure 2. MMR heterogeneity impairs tumorigenesis exclusively in immunocompetent animals

(A) *Mlh1*$^{+/+}$/*Mlh1*$^{-/-}$ mixed populations (100%/0%, 50%/50%, 20%/80%, and 0%/100%) were injected simultaneously in immunocompetent (BALB C) and immunocompromised (NOD SCID) mice (5 × 10^5 cells per mouse). (B) Tumor volumes (mm^3) of single mice are represented. NOD SCID tumor volumes are indicated at day of sacrifice (day 14). BALB C tumor volumes are depicted at day in which 100% *Mlh1*$^{+/+}$ were sacrificed (day 17). The black dash represents the mean of each group. Tumor growth was followed until ethical endpoints. The number of tumor free mice at the end of the experiment/total number of mice is reported for each group. This experiment was performed once. Statistical significance was evaluated by Mann-Whitney test: ***p = 0.0001; ****p < 0.0001. See also Figure S2.

The growth delay of MMR heterogeneous tumors depends on a competent immune system

To assess whether the growth delay observed upon transplantation of MMR heterogeneous population was dependent on the immune response, we performed parallel injections of *Mlh1*$^{+/+}$/*Mlh1*$^{-/-}$ heterogeneous populations (100%–0%, 20%–80%, 50%–50%, 0–100%, respectively) in immunocompetent (BALB C) and immunocompromised (NOD SCID) mice (Figure 2A). In this experiment we added 50% *Mlh1*$^{+/+}$ 50% *Mlh1*$^{-/-}$ cell mix to investigate whether also a reduced fraction of MMRd cells (compared with an 80% MMRd fraction tested in Figure 1) was able to affect tumor growth. Notably, a fraction of the immunocompetent mice injected with populations containing at least 50% of MMRd cells rejected the tumor completely (Figure 2B). In immunocompromised mice, regardless of the composition of the injected populations, cells engrafted and rapidly expanded leading to sacrifice for ethical reasons in less than 3 weeks (Figures 2B and S2).

The local immune microenvironment is responsible for immune surveillance of MMR heterogeneous tumors

Results presented in Figures 1 and 2 show that a subset of the immunocompetent mice injected with MMR heterogeneous cell populations did not develop tumors. To functionally address how MMRd and MMRp cells interacted with the immune system, we assessed whether proximity between the two cellular types were required to elicit effective immune responses. For this purpose, we injected 100% *Mlh1*$^{+/+}$ cells in one flank and 100% *Mlh1*$^{-/-}$ cells in the opposite flank of a group of mice and monitored tumor growth over time (Figure 3A). A total amount of 5 × 10^5 cells (2.5 × 10^5 cells for each genotype) were injected, so that the total amount of injected cells per mouse was consistent with that used in previous experiments. As shown in Figure 3B, tumors were visible in all flanks of animals injected with *Mlh1*$^{+/+}$ cells, independent of the presence of a *Mlh1*$^{-/-}$ mass in the opposite flank. These experiments indicate that immune responses elicited by MMRd cells at the site of tumor injection are responsible for the elimination of MMRd and MMRp tumor cells in the same local microenvironment, while immune response elicited locally by MMRd tumor cells is not effective against MMRp tumor cells injected at a distant site.

Immune evasion of MMR heterogeneous tumors is driven by the MMR-proficient fraction

As discussed above, MMR heterogeneous tumors trigger immune surveillance, which in some instances leads to complete tumor rejection. However, tumors rapidly progress in a fraction of the immunocompetent mice (Figure 2B). To address the mechanism that led to the loss of immune control, we explanted tumors that grew (escaped) in immunocompetent mice (Figures 2, 4A, and S2) and extracted gDNA from the entire sample. A ddPCR assay was deployed to assess with accuracy the *Mlh1* $^{+/+}$ and *Mlh1* $^{-/-}$ fractions based on defined sequence variations at the *Mlh1* locus generated by genome editing (Figure S1B). We found that the percentage of the MMRp fraction detected after *in vivo* growth was much higher than in the samples before the injection. Essentially, the tumors that eventually grew were composed mainly of *Mlh1*$^{+/+}$ cells, and, in some cases, *Mlh1*$^{-/-}$ cells were completely absent (Figure 4B).

Immune cell profiling of the MMR heterogeneous tumor microenvironment

To address whether the presence of *Mlh1*$^{-/-}$ cells was sufficient to increase immune cells infiltration in MMRd/MMRp heterogeneous tumors, we injected *Mlh1*$^{+/+}$/*Mlh1*$^{-/-}$ cells at different

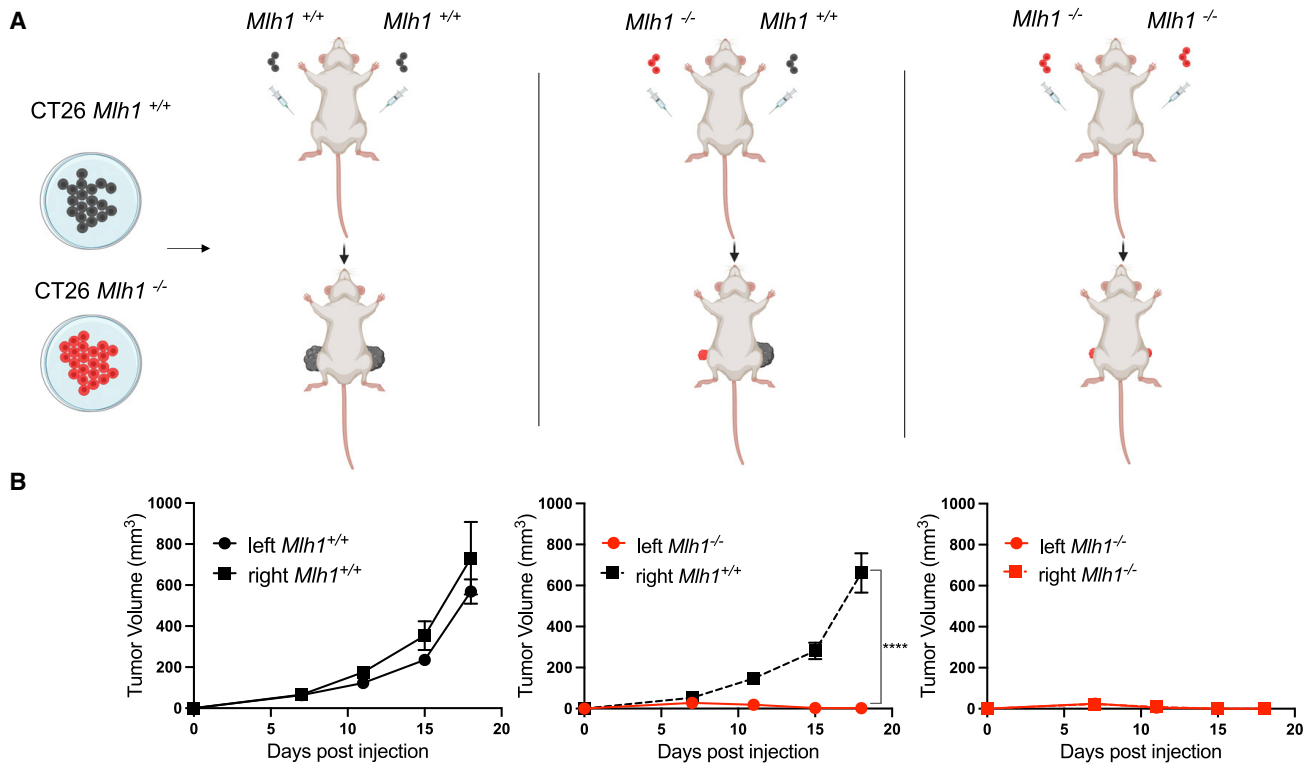

Figure 3. Injection of MMRp and MMRd tumors in contralateral flanks of individual mice

(A) Graphical summary: 100% *Mlh1*$^{+/+}$ and 100% *Mlh1*$^{-/-}$ CT26 cells were simultaneously injected in the two flanks of the same animal (BALB C). Different combinations were studied (left *Mlh1*$^{+/+}$right *Mlh1*$^{+/+}$; left *Mlh1*$^{-/-}$right *Mlh1*$^{-/-}$; left *Mlh1*$^{-/-}$ right *Mlh1*$^{+/+}$). A total of 2.5 × 10^5 cells were injected in each flank to parallel the number of cells per mice used in the other experiments. (B) Tumor growth was monitored twice a week and is reported in the graph as average of tumor volumes (mm^3) ± SEM. Each experimental group was composed of 12 animals, with the exception of left *Mlh1*$^{-/-}$ right *Mlh1*$^{-/-}$ group (n = 11). This experiment was performed once. Statistical significance was evaluated by Mann-Whitney test: ****p < 0.0001.

ratios (Figure S3A) in immunocompetent animals and explanted tumors once their growth had stabilized (approximately day 13). In mice injected with 100% *Mlh1*$^{-/-}$ and 20% *Mlh1*$^{+/+}$ 80% *Mlh1*$^{-/-}$ cells, tumors did not reach an appropriate size for immune phenotyping analysis. After isolation of tumor infiltrating mononuclear cells, we assessed by flow cytometry the frequency of CD8$^+$ T, CD4$^+$ T, natural killer, B cells, macrophages, γδ T, and regulatory T cells (Treg). Tumors containing 50% MMRp and 50% MMRd fractions displayed increased percentage of CD8$^+$ T cells compared with 100% *Mlh1*$^{+/+}$tumors, and even tumors containing only 20% of *Mlh1*$^{-/-}$ cells recruited more CD8$^+$ T cells than control tumors. This increase of CD8$^+$ T cells was accompanied by an increase of Treg cells[28] in 50% *Mlh1*$^{+/+}$ *Mlh1*$^{-/-}$ group and a reduction of B cells (Figure 5A). This suggests that the presence of a relatively small fraction of MMRd cells can affect tumor immunoediting.

MMR heterogeneity boosts γδ T cell reactivity toward *Mlh1*$^{+/+}$ cells

To address mechanisms of immune control exerted on MMR heterogeneous tumors, we assessed effector function of lymphocytes (CD8$^+$ T, CD4$^+$ T, γδ T) by coculturing them with *Mlh1*$^{+/+}$ or *Mlh1*$^{-/-}$ tumor cells (Figures 5B and 5C). Briefly, CT26 tumor cells (100% *Mlh1*$^{+/+}$ or 50% *Mlh1*$^{-/-}$ 50% *Mlh1*$^{+/+}$) were injected in immunocompetent BALB C mice. Since the size of the heterogeneous tumors did not allow to collect enough tumor-infiltrating lymphocytes, peripheral blood mononuclear cells (PBMCs) were purified on day 13 from mouse blood and co-cultured with either *Mlh1*$^{+/+}$ or *Mlh1*$^{-/-}$ tumor cells. Lymphocyte effector function was assessed by intracellular interferon (IFN)-γ protein expression after 5 h of co-culture (Figures 5B, 5C, and S3B). CD8$^+$ T cells from *Mlh1*$^{+/+}$ *Mlh1*$^{-/-}$ tumor-bearing mice were activated to produce IFN-γ by *Mlh1*$^{-/-}$ tumor cells but not by *Mlh1*$^{+/+}$ cells (Figures 5B and 5C), and this result confirmed the reactivity of CD8$^+$ T cells against *Mlh1*$^{-/-}$ tumors previously described.[27] Interestingly, among the different lymphocyte types from PBMC of mice harboring 50% *Mlh1*$^{-/-}$ 50% *Mlh1*$^{+/+}$ tumors, the γδ T cells displayed the highest and most consistent effector function against *Mlh1*$^{+/+}$ cells, while we observed only a modest activation of γδ T cells from 100% *Mlh1*$^{+/+}$ tumor-bearing mice (Figure 5B). The effector function of γδ T cells toward *Mlh1*$^{-/-}$ tumor cells was observed also in PBMC isolated from naive mice, suggesting that the activation was not tumor dependent (Figures 5B and 5C).

To address the functional role of CD8$^+$ T and γδ T cells in an MMR heterogeneous tumor response, we depleted these cells with monoclonal antibodies *in vivo* (Figures 5D and 5E). After CD8$^+$ T cell depletion in immunocompetent mice, there was an impairment of the response against 50% *Mlh1*$^{-/-}$ 50% *Mlh1*$^{+/+}$ tumors. Indeed, tumor growth was faster in CD8$^+$T -depleted mice compared with untreated controls (Figures 5D

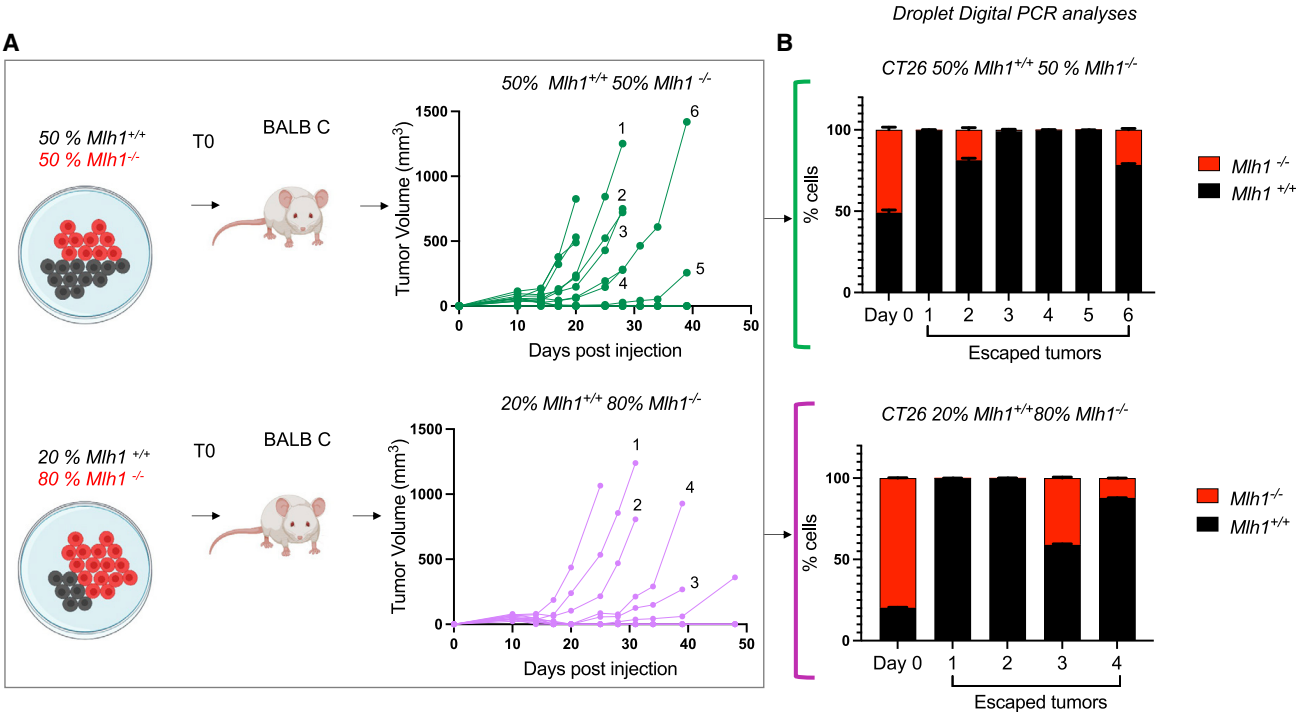

Figure 4. The MMRp component drives immune evasion of MMR heterogeneous tumors

Tumor escaped from immune control of BALB C during the experiment reported in Figures 2 and S2 are depicted as single mouse tumor growth and analyzed at molecular level.

(A) 50% *Mlh1*$^{+/+}$ 50% *Mlh1*$^{-/-}$ and 20% *Mlh1*$^{+/+}$ 80% *Mlh1*$^{-/-}$ CT26 cell populations were subcutaneously injected in immunocompetent BALB C mice (see Figures 2 and S2) and the growth is reported in the graph as single tumor volumes (mm^3). Tumors were allowed to expand until ethical endpoint, then they were explanted.

(B) DNA was extracted from the heterogeneous cell populations before the injection (day 0) and then from the whole tumor mass grown in randomly selected animals (n = 6 for 50% *Mlh1*$^{+/+}$ 50% *Mlh1*$^{-/-}$ group; n = 4 for 20% *Mlh1*$^{+/+}$ 80% *Mlh1*$^{-/-}$ group). Two or three samplings for each tumor were analyzed by ddPCR to determine the *Mlh1*$^{-/-}$ and *Mlh1*$^{+/+}$ cell fractions. Data are represented as average % of cells ± standard deviation for each tumor. The experiment was performed once. See also Figure S1B.

and 5E). Treatment with monoclonal antibody anti-γδ T cells gave more heterogeneous responses; in nine mice, tumors progressed and in three mice tumors were rejected (Figure 5E).

We then assessed the *Mlh1*$^{+/+}$ and *Mlh1*$^{-/-}$ fractions in tumors that grew in mice that were depleted of CD8$^+$ T or γδ T cells. We observed that, in mice lacking CD8$^+$ T cells, all outgrown tumors were composed mainly by MMRd cells, confirming that CD8$^+$ T cells are very effective against *Mlh1*$^{-/-}$ cells (Figure 5F). Interestingly, tumors that escaped after the depletion of γδ T cells were composed mainly of MMRp cells, thus suggesting that, in this case, tumor growth is mainly due to a decrease in γδ T cell reactivity against *Mlh1*$^{+/+}$ cells (Figure 5F).

Overall, our findings show that both CD8$^+$ T and γδ T cells can control the growth of MMR heterogeneous tumors, but they possibly do it through different mechanisms; CD8$^+$ T cells should be very effective against *Mlh1*$^{-/-}$ cells and γδ T cells toward *Mlh1*$^{+/+}$ cells.

Treatment with the anti-cancer agents 6-thioguanine and TMZ increase the MMRd fraction and improves immune surveillance

We and others have previously shown that exposure to the alkylating agent TMZ can result in the selection of cells carrying altered MMR genes.[27,29,30] It has also been reported that MMRd cells are more resistant than their proficient counterpart to 6-thioguanine (6TG).[31] TMZ is approved for the treatment of multiple malignancies including glioblastoma, while 6TG is currently used in hematologic malignancies.[32,33] To assess the impact of TMZ and 6TG on our mouse cellular models, we performed a loss-of-function genetic screen using a custom pooled CRISPR library targeting 488 genes involved in DNA damage response (DDR) and repair pathways (Table S1). This approach allowed the identification of genes that, when disabled, lead to drug resistance in the mouse CRC CT26 cell model. A CT26 clone stably expressing Cas9 was infected with the DDR library at a low multiplicity of infection to ensure that cells were carrying a single lentiviral copy and to achieve approximately 500× coverage of each sgRNA. After puromycin selection, cells were treated with TMZ or 6TG at concentrations of 100 and 1 μM, respectively, for 14 days. Next, gDNA was extracted and sequenced by next-generation sequencing to determine the abundance of individual sgRNAs (Figure S4A). Several MMR genes including *Mlh1*, *Msh2*, *Msh6*, and *Pms2* were among the top significant hits conferring resistance to both compounds (Figures S4B and S4C). We reasoned that TMZ and 6TG could be used to select/enrich for MMRd fraction in a heterogeneous

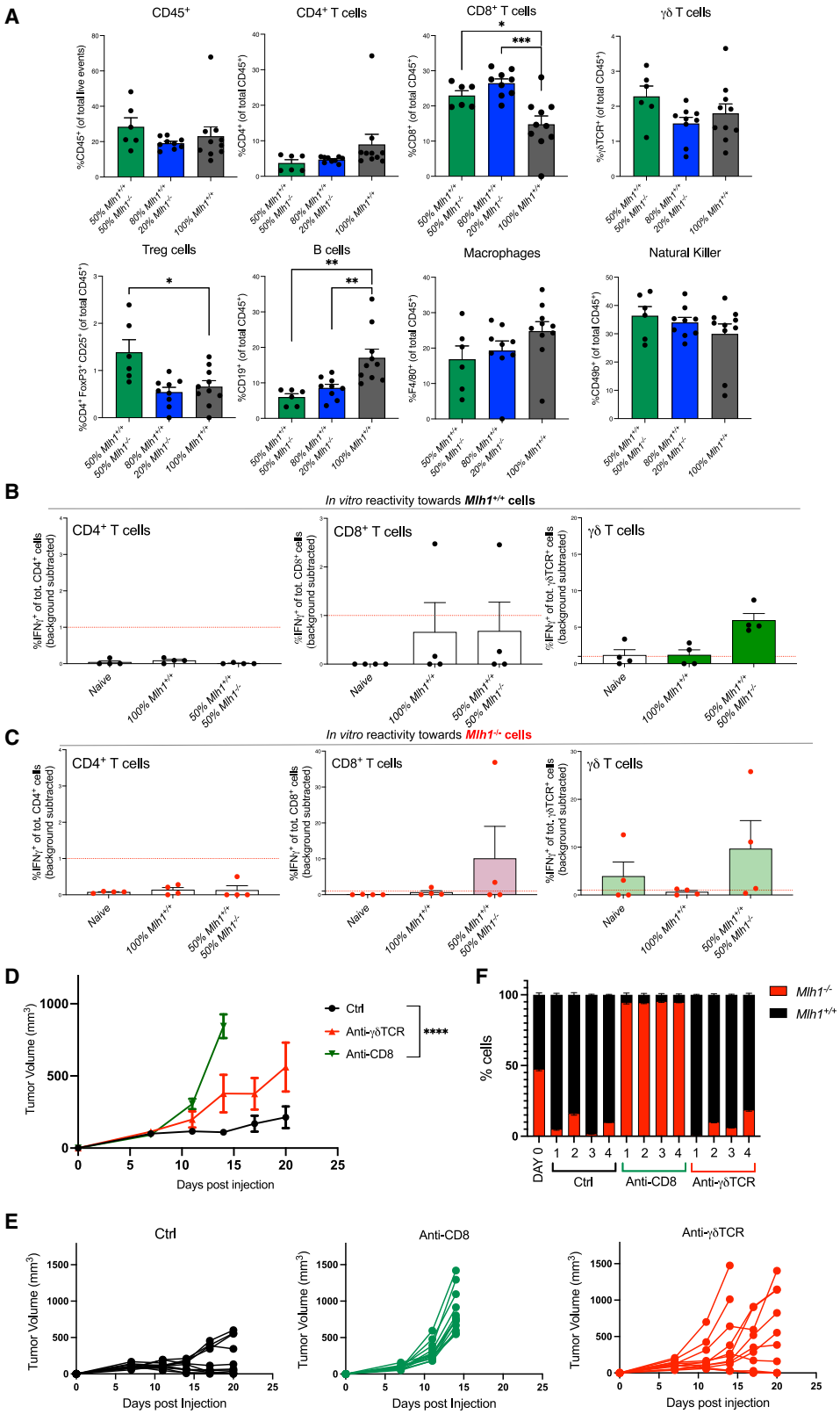

Figure 5. Immune profiling of MMR heterogeneous tumors reveals the involvement of CD8$^+$ and γδ T cells

(A) MMR heterogeneous tumors (100% *Mlh1*$^{+/+}$, 80% *Mlh1*$^{+/+}$ 20% *Mlh1*$^{-/-}$, 50% *Mlh1*$^{+/+}$ 50% *Mlh1*$^{-/-}$) were analyzed 13 days after injection in immunocompetent BALB C mice. Immune cell infiltrate was evaluated by flow cytometry. Percentages of CD8$^+$ T, CD4$^+$ T, γδ T (γδ-TCR$^+$), T reg (CD4$^+$ FoxP3$^+$ CD25$^+$), B (

(legend continued on next page)

cell population. We, therefore, treated an 80% *Mlh1*$^{+/+}$ 20% *Mlh1*$^{-/-}$ mixed population with both agents and analyzed their composition at different timepoints post treatment (Figure 6A). A substantial increase of the MMRd component was observed as early as 96 h after drug exposure (Figure 6B). Encouraged by these results, the experiment was repeated by treating a population composed of 99% of *Mlh1*$^{+/+}$ cells and only 1% of *Mlh1*$^{-/-}$ cells. After as early as 8 days of 6TG selection there was a remarkable reversal of the population composition that contained mainly *Mlh1*$^{-/-}$ cells (Figure 6C).

Finally, we investigated whether pharmacological selection of MMRd cells was effective also *in vivo*. First, we subcutaneously injected 80% *Mlh1*$^{+/+}$ 20% *Mlh1*$^{-/-}$ CT26 population in syngeneic mice; then, we treated animals with 6TG or DMSO vehicle. Subsequently, we determined tumor composition (fraction of *Mlh1*$^{-/-}$ *Mlh1*$^{+/+}$ cells) by ddPCR on gDNA extracted from the tumors (Figure 6D). We found that 6TG-treated tumors showed a strong enrichment of the MMRd component (Figure 6E).

These results indicate that the MSI/MMRd status of molecularly heterogeneous tumors can be modulated pharmacologically both *in vitro* and *in vivo*.

Next, we addressed whether approved chemotherapeutic agents might enrich the MMRd fraction in a model of heterogeneous tumors. To assess this, we treated a population of 80% *Mlh1*$^{+/+}$ 20% *Mlh1*$^{-/-}$ cells with 6TG or TMZ *in vitro* for 10 days (Figure 7A). As expected, after treatment with either drug, a strong increase of the *Mlh1*$^{-/-}$ fraction was observed (Figure 7B).

When injected in immunocompetent mice, populations of cells treated with 6TG and TMZ formed small masses or did not grow at all (Figures 7C and 7D). To assess whether this effect was immune driven or related to the exposure of cells to the drug, the experiment was performed in parallel in immunocompromised animals. Although 6TG and TMZ *in vitro* treatments affected the growth of the equivalent populations injected in immunocompromised mice (Figures 7C and 7D), all tumors eventually grew in immune deficient animals, while a large fraction of the immunocompetent animals remained tumor free (Figure 7D). These data suggest that TMZ and 6TG treatments affect tumor growth and that the efficacy of the drugs on MMR heterogeneous tumors is enhanced in immune competent mice.

Therapy with 6TG impairs the growth of tumors containing small fractions of MMR-deficient cells

We next assessed the *in vivo* impact of previously described anti tumoral compounds on heterogeneous tumors (Figure S5A). Since TMZ displayed unacceptable toxicity in mice, we administered 6TG to mice injected with variable fractions of MMRp and MMRd cells (Figure S5A). In tumors containing 100% *Mlh1*$^{+/+}$ cells, growth delay was observed upon 6TG treatment, while in a population composed of 50% *Mlh1*$^{+/+}$ 50% *Mlh1*$^{-/-}$, 6TG massively restricted tumor growth (Figure 8). After an initial progression, 6TG-treated tumors started to shrink, leading to almost complete regressions in all animals (Figures 8 and S5B). Intrigued by these results, we repeated the experiment starting from a population of 80% *Mlh1*$^{+/+}$ and 20% *Mlh1*$^{-/-}$. Notably, even if the fraction of MMRd cells was initially in the minority, 6TG treatment induced tumor regressions in most (8/10) of the animals (Figure 8). Relevant to possible therapeutic applications, responses were long lasting, and mice remained cancer free or displayed tumor stability for at least 120 days (data not shown), after which they were sacrificed. These data indicate that pharmacological modulation of the MMR status can foster immune surveillance of MMR heterogeneous tumors.

DISCUSSION

The status of the MMR machinery is a key determinant for immunotherapy in CRC. Patients diagnosed with MMRd tumors are usually greatly sensitive to ICB,[10,11,34] while those MSS/MMRp are mostly unresponsive.[9] Intriguingly, in a rare but peculiar subset of CRC and other cancer types, expression of MMR proteins can be heterogeneous, with tumors containing variable fractions of MMRp and MMRd cells.[20,22]

The clinical relevance of MMR heterogeneity is not limited to the fraction of CRCs displaying MMR heterogeneity, since the coexistence of MMRp and MMRd subclonal components can be modulated by pharmacological treatments, as recently highlighted by the ARETHUSA trial.[26] Notably, in this proof-of-concept study, drug-induced emergence of subclonal MMR alterations promoted clinical benefit upon pembrolizumab treatment in initially MSS CRCs. Of note, in one ARETHUSA patient, the detection of subclonal *MSH6* mutations was paralleled by a

CD19$^+$), natural killer cells (CD49b$^+$), and macrophages (F4/80$^+$), were calculated normalizing the absolute number of each population with the viable CD45$^+$ fraction. The total amount of CD45$^+$ alive cells is reported. Data are represented as average % ± standard error of the mean. The experiment was performed once. Tumors with insufficient material for immunophenotypical characterization were excluded from the analyses; n = 10 for 100% *Mlh1*$^{+/+}$ group, n = 9 for 80% *Mlh1*$^{+/+}$ 20% *Mlh1*$^{-/-}$ group, n = 6 for 50% *Mlh1*$^{+/+}$ 50% *Mlh1*$^{-/-}$ group. Statistical significance for each mixed population compared to the 100% *Mlh1*$^{+/+}$ control group was calculated by one-way ANOVA: *p < 0.05 **p < 0.005 ***p < 0.0005; (B) *Ex vivo* reactivity assays; CT26 100% *Mlh1*$^{+/+}$ and 50% *Mlh1*$^{+/+}$ 50% *Mlh1*$^{-/-}$ were injected in immunocompetent BALB C mice. On day 13, mice were sacrificed and blood was taken. PBMCs were isolated and cocultured with *Mlh1*$^{+/+}$or *Mlh1*$^{-/-}$ separately (ratio PBMCs to tumor cells of 1:1). PBMCs harvested from naive mice were used as controls. IFN-γ expression was analyzed by flow cytometry as marker of activation after 5 h of coculture. The analyses of IFN-γ$^+$ CD8$^+$ T, IFN-γ$^+$ CD4$^+$ T, IFN-γ$^+$ γδ T cells obtained from the coculture with *Mlh1*$^{+/+}$ cells or (C) *Mlh1*$^{-/-}$ cells is reported. At least three biological replicates were performed for each of the immune cell populations. Each dot represents a single biological replicate. Only conditions in which at least two biological replicates were above the threshold of 1% of IFNγ$^+$ cells (after background subtraction) were considered specifically activated. Mean ± standard error of the mean is reported (D) CT26 50% *Mlh1*$^{-/-}$ 50% *Mlh1*$^{+/+}$ cells were injected in immunocompetent BALB C mice treated with depleting antibody for CD8$^+$ T cells or γδ T cells. Twelve mice per group were used. Untreated mice served as control. Depleting CD8$^+$ T cell antibody was given according to the following schedule: 400 μg at the day of the injection, 200 μg at the day 2, and then every 3 days after injection. Depleting γδ T cell antibody was administered according to the following schedule: 400 μg 2 days and 1 day before the injection, 400 μg at days 3 and 6 after injection followed by 400 μg every 7 days. Tumors were measured twice a week and volumes are reported as average tumor volume (mm^3) ± standard error of the mean; Mann-Whitney statistical analyses was performed, ****p < 0.0001. (E) Single mice graphs of the experiment shown in Figure 5D are reported. (F) gDNA was extracted from four immune escaped tumors per arm (randomly selected), and ddPCR analyses was performed to determine the *Mlh1*$^{+/+}$ *Mlh1*$^{-/-}$ cell content. Two or three sampling for each tumor were analyzed. Day 0 indicates the day of tumor cell injection. Data are represented as average % of cells ± standard deviation for each tumor. The experiment was performed once. See also Figure S3.

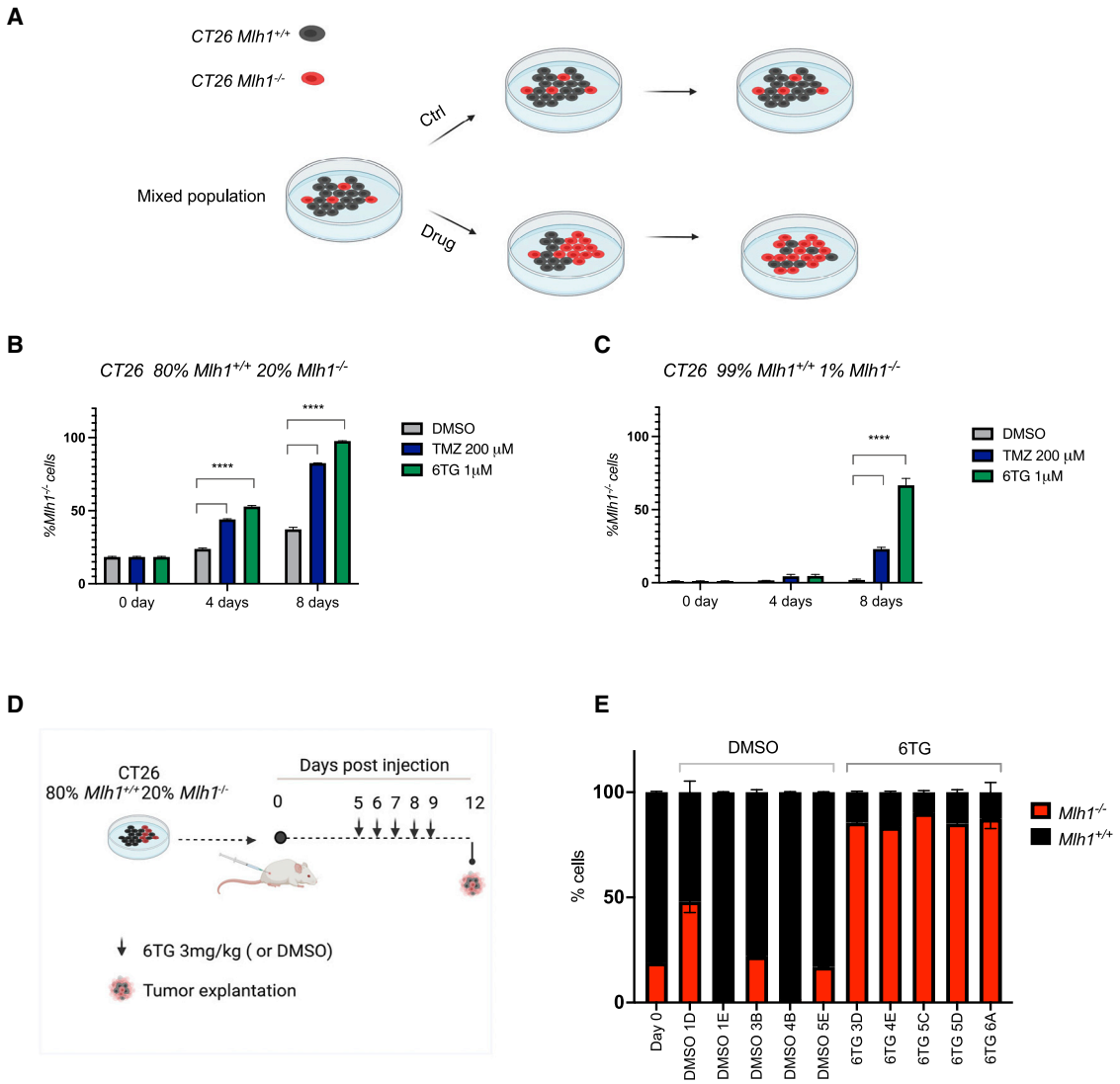

Figure 6. *In vitro* pharmacological treatments of MMR heterogeneous populations

(A) *Mlh1*$^{-/-}$ and *Mlh1*$^{+/+}$ mixed population were plated (1 × 10^5 per well). After 24 h, cells were treated with TMZ 200 μM, 6TG 1 μM, or DMSO. gDNA was extracted after 4 and 8 days and ddPCR analyses were performed. (B) The 80% *Mlh1*$^{+/+}$ 20% *Mlh1*$^{-/-}$ and (C) 99% *Mlh1*$^{+/+}$ 1% *Mlh1*$^{-/-}$ populations were tested. Data are presented as average % of *Mlh1*$^{-/-}$ cells ± standard deviation. Experiment was performed three times, and each condition represents the average of a technical triplicate. This figure reports one representative experiment. Two-way ANOVA (multiple comparisons) was used for statistical analyses: ****$p < 0.0001$.

(D) CT26 *Mlh1*$^{+/+}$/*Mlh1*$^{-/-}$ mixed population (80%/20%) was injected subcutaneously in immunocompetent BALB C mice. On day 5 after injection, intraperitoneal treatment with 6TG 3 mg/kg was initiated and repeated daily until day 9. On day 12 after injection, mice were sacrificed, tumors were harvested and gDNA was extracted.

(E) ddPCR to determine *Mlh1*$^{+/+}$/*Mlh1*$^{-/-}$ cell percentage was performed. Results are reported in the bar graph. Two or three sampling for each tumor were analyzed. Day 0 represents the percentage of *Mlh1*$^{+/+}$ *and Mlh1*$^{-/-}$ cells in the population at day of the injection. Data are represented as average % of cells ± standard deviation for each tumor. The experiment was performed once, n = 5 per group. See also Figure S4.

prolonged disease stabilization upon pembrolizumab treatment.[26] Tumor progression was observed when the MSH6 mutation was no longer detectable in the plasma of the patient, suggesting that the MMRd component sustained the immune response while the MMRp subclone was dominant during immune evasion.

Whether and how MMR heterogeneity leads to a modified tumor immune microenvironment and affects immune surveillance is largely unknown. Here, we experimentally addressed this question by mixing isogenic *Mlh1*$^{+/+}$ (MMRp) and *Mlh1*$^{-/-}$ (MMRd) CRC cells to generate MMR heterogeneous tumors in mice. We found that the cohabitation of MMRp and MMRd cells promotes immune surveillance. Notably, the effectiveness of the immune response was proportional to the fraction of MMRd cells present in the tumor mass. Indeed, some tumors in which the MMRd fraction was as low as 50% did not grow in immunocompetent mice, suggesting that MMRd cells triggered effective immune responses also toward their MMRp counterparts.

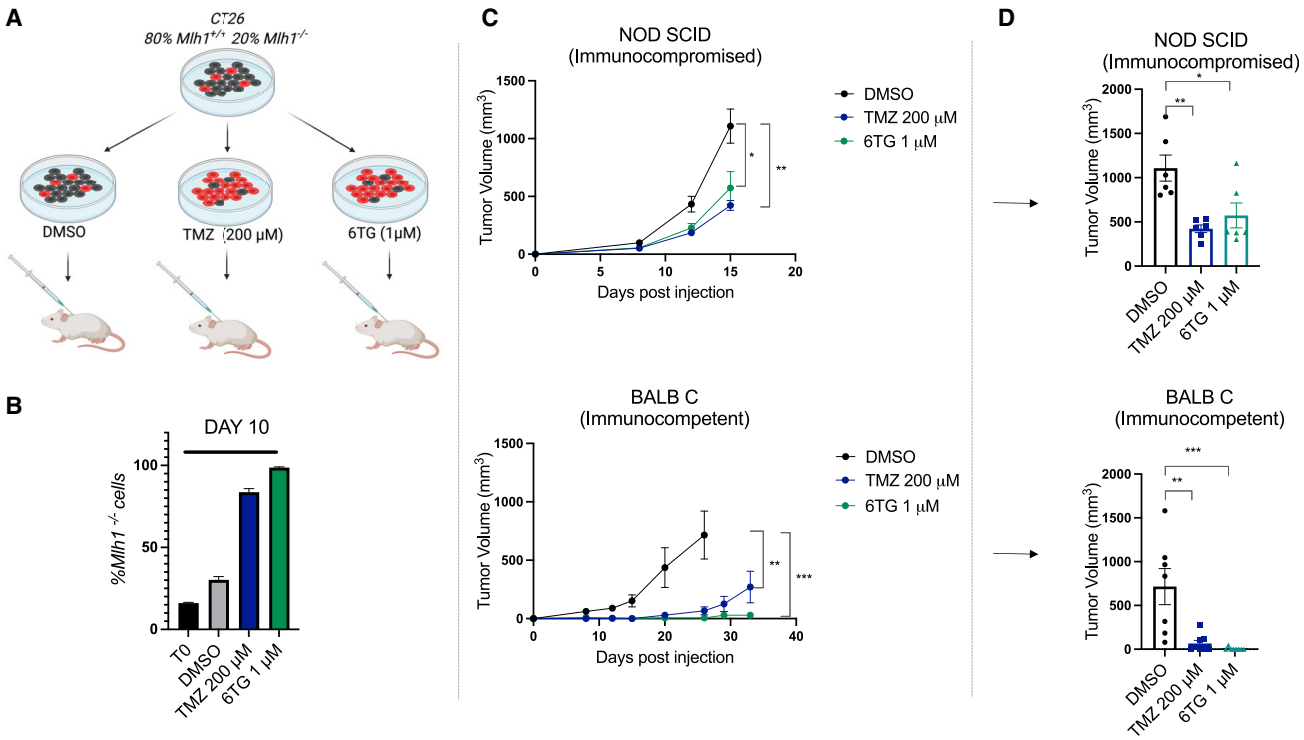

Figure 7. Pharmacological selection of MMRd cells increases immune surveillance *in vivo*

(A) Experimental scheme: CT26 (80% *Mlh1*$^{+/+}$ 20% *Mlh1*$^{-/-}$) cells were plated in 10-cm dishes (1 × 10^5 cells, T0). After 24 h, drug selection (TMZ 200 μM, 6TG 1 μM, or DMSO) was administered for 10 days.

(B) Percentage of *Mlh1*$^{-/-}$ cells after 10 days of drug treatment *in vitro*. To define the percentage of knock out cells, gDNA was extracted and analyzed for *Mlh1*$^{-/-}$ content by ddPCR. Two sampling for each condition were tested. Data are represented as average % of *Mlh1*$^{-/-}$ cells ± standard deviation. (C) Mixed populations obtained from (A) were injected in NOD SCID (immunocompromised) and BALB C (immunocompetent) mice (5 × 10^5 cells per mouse). Tumor growth was monitored and is reported in the graph as average of tumor volumes (mm^3) ± standard error of the mean. (D) Tumor volumes (mm^3) of single mice on day 15 (NOD SCID, day of sacrifice) and 26 (BALB C, day of sacrifice of DMSO arm) are reported. Data are represented as average tumor volumes (mm^3) ± standard error of the mean, while each dot represents one single mouse value. The number of tumor free BALB C mice on day 26 were none of eight for the DMSO group, four of eight for the TMZ group, and seven of eight for the 6TG group. NOD SCID experimental groups n = 6; BALB C experimental groups n = 8. The experiment was performed once. Statistical significance was evaluated by Mann-Whitney test: *p < 0.05, **p < 0.005, ***p < 0.0005.

The characterization of tumor infiltrating immune cells in MMR heterogeneous tumors revealed MMRd-driven modulation of the immune microenvironment. A small percentage (20%) of *Mlh1*$^{-/-}$ cells was sufficient for effective recruitment of CD8$^+$ T cells; furthermore, MMRd cells were also able to induce a specific γδ T cells reactivity toward the *Mlh1*$^{+/+}$ component in cancers that would be classified as MSS according to standard diagnostic practice. Rejection of MMR heterogeneous tumors was observed only when the MMRd and MMRp fractions were present at the same site, suggesting a key role of the local microenvironment.

To understand the mechanism underlying the outgrowth of MMR heterogeneous tumors, we assessed their composition and found that the MMRp fraction drives immune escape, limiting immune surveillance and regenerating tumors that were prevalently MMRp. Indeed, in all cases, the amount of *Mlh1*$^{+/+}$ cells increased over time, and this component became dominant also in tumors initially harboring an excess (approximately 80%) of *Mlh1*$^{-/-}$ cells. These data revealed that, at least in our model, MMRp cells might be responsible for immune evasion. Moreover, the risk of tumor outgrowth increases with the percentage of MMRp cells in the mixed population.

Interestingly, we found that the enrichment of a subclonal MMRd component through 6TG or TMZ, two anti-cancer drugs regularly used in the clinic, promoted immune surveillance. *In vitro* treatment of a mixed population with 6TG or TMZ rapidly increased the MMRd fraction. More important, we report that, also *in vivo*, 6TG leads to selection of MMRd cells. In addition, cells treated *in vitro* with 6TG or TMZ and then injected in immunocompetent mice triggered an immune response stronger than that induced by the untreated population.

We also investigated whether treatment with 6TG *in vivo* increases immune surveillance of MMR heterogeneous tumors. In a CRC cancer murine model, *in vivo* 6TG treatment fostered immune surveillance and restricted immune evasion, hindering the outgrowth of the MMRp subclonal fraction. Indeed, upon 6TG treatment, MMR heterogeneous tumors were eliminated. We speculated that an increased percentage of MMRd cells results in stronger activation of the immune system, leading to complete eradication of MMR heterogeneous cancers.

The CRC mouse model system we used has several limitations. First, MMR heterogeneous tumors were generated mixing *Mlh1*$^{+/+}$ and *Mlh1*$^{-/-}$ isogenic cells, which only partially recapitulates the human condition in which the dynamics of MMR

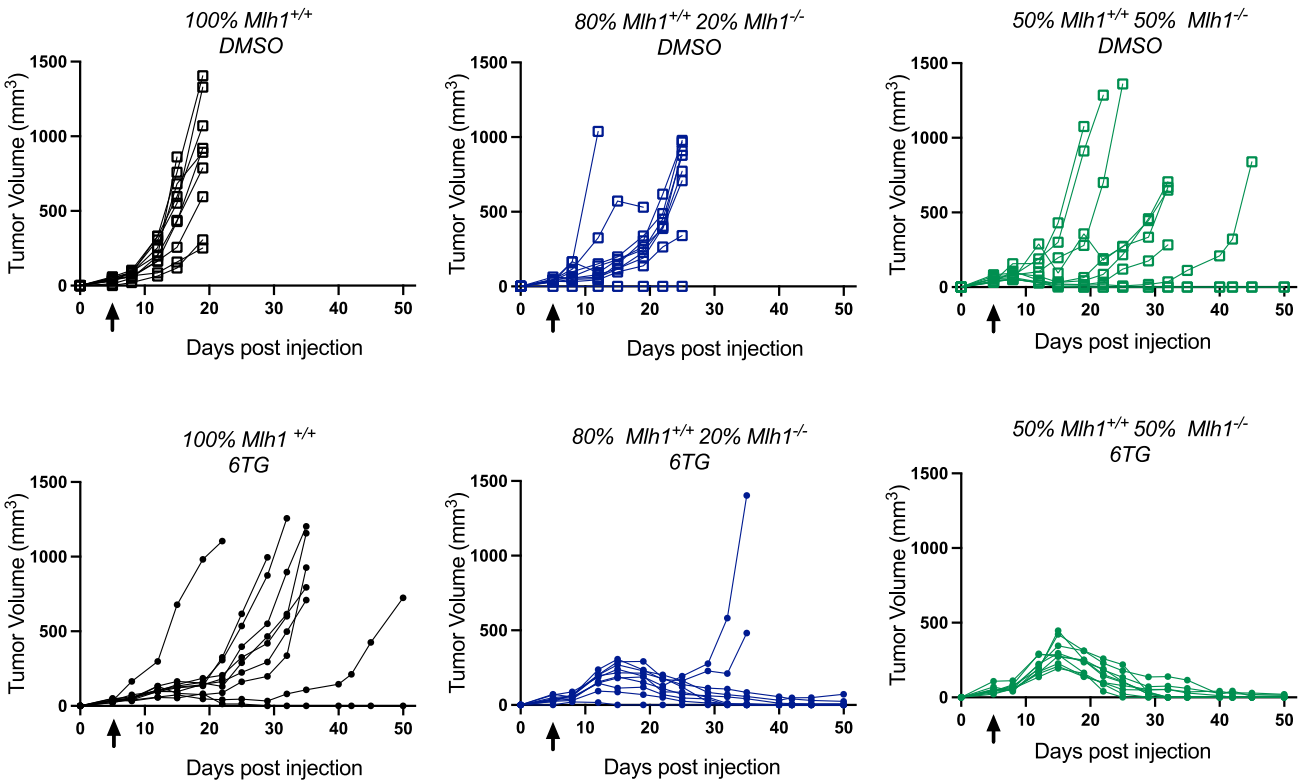

Figure 8. *In vivo* treatment with 6TG induces regression of MMR heterogeneous tumors

CT26 MMR heterogeneous populations (100% *Mlh1*$^{+/+}$, 80% *Mlh1*$^{+/+}$20% *Mlh1*$^{-/-}$, 50% *Mlh1*$^{+/+}$ 50% *Mlh1*$^{-/-}$) were injected in immunocompetent BALB C mice (5×10^5 cells per mouse). Five days after injection, mice were treated with 6TG 3 mg/kg for 5 days. The arrows indicate the start of 6TG treatment. DMSO treated mice served as controls. Single tumor volumes (mm^3) until day 50 (the day of sacrifice of the last growing tumor) are reported. Tumor-free mice and mice with small stabilized tumors were followed for at least 120 days after injection. Each experimental group was composed of 10 animals. The experiment was performed once. See also Figure S5.

heterogeneous status are likely complex and remain largely unknown. Second, a murine model encompassing two isogenic derivatives does not recapitulate the disease heterogeneity observed in human cancers, in which several subpopulations coexist. Notwithstanding the limits of the MMR model presented here, this proof-of-concept study experimentally highlights the impact of MMR heterogeneity on tumor immune surveillance. Our findings put MMR heterogeneity at center stage in relation to immunotherapy in CRC patients for at least two reasons. From a translational point of view, our work suggests that to intercept a potentially overlooked subset of CRC patients that could benefit from ICB therapies in virtue of their tumor MMR heterogeneity, the MMR status should be tested in multiple regions of the patient's surgical specimen(s). Indeed, this fraction of patients is of unknown magnitude, as previously pinpointed by Tachon et al., because of the diagnostic practice of testing a single tumor block, a suboptimal procedure for the identification of MMR heterogeneous cases.[24] Accordingly, Chapusot et al. identified eight cases with discordant results between IHC for MMR proteins and molecular testing, and only by analyzing multiple blocks of the same tumors were they able to demonstrate heterogeneity in the expression of MMR proteins.[22] These findings support the notion that the true rate of MMR heterogeneity is currently underestimated and that only the analysis of multiple intra-tumoral regions of the same tumor could uncovers the actual extent of this phenomenon. The clinical relevance of MMR heterogeneity would in any case apply also if the MMR heterogeneous patient population turns out to be small, as highlighted by the recent results of our ARETHUSA Trial.

The therapeutic implications of MMR heterogeneity in CRC and other cancer types are still largely unknown. Loupakis et al. reported prolonged disease stabilization under ICB in a mCRC patient tumor with both MMRp and MMRd components,[20] whereas a study on metastatic gastric cancers suggested that MMR heterogeneity might predispose to pembrolizumab resistance.[18] Our findings give experimental support to a suggestive single patient narrative and advocates that a pharmacologically forced selection for MMRd cells could be harnessed, at least conceptually, to unleash immune surveillance of MSS CRC tumors in patients. TMZ and 6TG are standard of care for, respectively, glioblastoma and childhood acute lymphoblastic leukemia; consequently, both drugs have a well-known safety profile and could be accessed off label. Thus, they could be exploited to prime MMR tumor for potential ICB response in a proof-of-concept trial similar to ARETHUSA.[35–38] Indeed, several reports from primary tumors with different histology highlighted that MMR deficiency is one of the key mechanisms of secondary resistance to 6TG or TMZ in clinical practice.[29,39] Accordingly, the ARETHUSA study recently

demonstrated that priming with TMZ can induce alterations in MMR genes, thus sensitizing O-6-methylguanine-DNA methyltransferase methylated MMRp mCRC to pembrolizumab.[26] The proof-of-concept clinical findings in ARETHUSA are supported by the results of the MAYA study, which showed that the empirically combination of TMZ with a double ICB achieved a remarkable 45% response rate in MMRp mCRC.[40] Collectively, these clinical studies suggest that MMR heterogeneity can also be pharmacologically induced and support the innovative design of additional trials.

In summary, our results indicate that genetic and/or pharmacological modulation of the DNA MMR machinery can trigger immune surveillance of MMR heterogeneous tumors and modulate cancer immune environment. The finding that conversion of immunologically "cold" into "hot" tumors is feasible could lead to increasing the fraction of patients eligible for ICB[41] and has implications for the rational design of clinical trials targeting tumors recalcitrant to immunotherapies.

STAR★METHODS

Detailed methods are provided in the online version of this paper and include the following:

- KEY RESOURCES TABLE
- RESOURCE AVAILABILITY
  - Lead contact
  - Materials availability
  - Data and code availability
- EXPERIMENTAL MODEL AND SUBJECT DETAILS
  - Mouse cell line
  - Animal studies
- METHOD DETAILS
  - Gene editing
  - Mouse treatments
  - Western Blot analyses
  - Genomic DNA extraction
  - Droplet digital PCR detection
  - *In vitro* enrichment assay
  - Immunophenotyping
  - *In vitro* reactivity
  - DNA damage response (DDR) library design and lentiviral production
  - Library sequencing and bioinformatic analysis of NGS data
- QUANTIFICATION AND STATISTICAL ANALYSIS

SUPPLEMENTAL INFORMATION

Supplemental information can be found online at https://doi.org/10.1016/j.ccell.2022.12.003.

ACKNOWLEDGMENTS

The authors thank members of the Molecular Oncology laboratory at Candiolo Cancer Institute, FPO – IRCCS and Neophore LTD staff for critically reading the manuscript. We also thank Dr M.L. Sarnicola, Dr M.C. Crosti, and Dr D. Manganaro for help with flow cytometry experiments. The research leading to these results has received funding from FONDAZIONE AIRC under 5 per Mille 2018 - ID. 21091 program – P.I. Bardelli Alberto (A. Bardelli) and Group Leaders Federica Di Nicolantonio (F.D.N.), Sergio Abrignani (S.A.), Caterina Marchiò (C.M.) and Silvia Marsoni (S.M.); AIRC under IG 2018 - ID. 21923 project – P.I. Bardelli Alberto (A.Bardelli); International Accelerator Award, ACRCelerate, jointly funded by Cancer Research UK (A26825 and A28223), FC AECC (GEACC18004TAB) and AIRC (22795); IMI contract n. 101007937 PERSIST-SEQ; Grant from University of Torino Ricerca Locale 2017 (F.D.N). The project leading to this application has received funding from the European Research Council (ERC) under the European Union's Horizon 2020 research and innovation program (grant agreement No 101020342). G.G. was supported by FPRC 5xmille 2017 Ministero Salute PTCRC-Intra 2020 (REGENERATION-YIG 2020 project) and by AIRC MFAG 2020 Grant-ID 24604-PI Giovanni Germano (G.G.). V.A. was supported by a AIRC fellowship for Italy. Images were generated with Biorender.com

AUTHOR CONTRIBUTIONS

V.A., G.G., and A.Bardelli conceived the study. V.A., G.G., and R.C. performed animal experiments. V.A., B.M., S.L., F.P., C.M.C, E.B., and A.Bartolini conduced the *in vitro* experiments and analyzed data. S.L performed gene-editing experiments. G.R. and G.C. conducted bioinformatics data analyses. C.M.C, V.A, and G.G performed acquisition and analysis of flow cytometry samples. S.A, C.T., G.G., and C.M.C critically revised immunological data interpretation. V.A, G.G., and A.Bardelli wrote the manuscript. S.A., G.M., C.M, F.D.N., M.C.A., E.B., and S.M. critically revised the manuscript. A.Bardelli, G.G., F.D.N., and V.A. supervised the study. All the authors read and approved the final manuscript.

DECLARATION OF INTERESTS

A.Bardelli served in a consulting/advisory role for Illumina, Inivata and Guardant Health. The transfer of certain materials to third parties is subject to terms contained within license and intellectual property agreements held between NeoPhore, the University of Turin, A.Bardelli and G.G. A.Bardelli and G.G. are cofounders and shareholders of NeoPhore limited. S.A. is a cofounder and shareholder of CheckMab SRL. A.Bardelli is a member of the scientific advisory board of Neophore, Inivata, and Roche Genentech CRC Advisory Board. A. Bardelli reports grants/research support from Neophore, AstraZeneca, and Inivata. C.M. reports personal consultancy fees from Bayer, Roche and Daichii Sankyo-AstraZeneca outside the scope of the present work. G.M. received honoraria from COR2ED outside the scope of the present work. The remaining authors declares no conflict of interest.

Received: January 8, 2022
Revised: March 23, 2022
Accepted: December 6, 2022
Published: December 29, 2022

REFERENCES

1. Germano, G., Amirouchene-Angelozzi, N., Rospo, G., and Bardelli, A. (2018). The clinical impact of the genomic landscape of mismatch repair-deficient cancers. Cancer Discov. *8*, 1518–1528. https://doi.org/10.1158/2159-8290.CD-18-0150.
2. Jiricny, J. (2006). The multifaceted mismatch-repair system. Nat. Rev. Mol. Cell Biol. *7*, 335–346. https://doi.org/10.1038/nrm1907.
3. Turajlic, S., Litchfield, K., Xu, H., Rosenthal, R., McGranahan, N., Reading, J.L., Wong, Y.N.S., Rowan, A., Kanu, N., Al Bakir, M., et al. (2017). Insertion-and-deletion-derived tumour-specific neoantigens and the immunogenic phenotype: a pan-cancer analysis. Lancet Oncol. *18*, 1009–1021. https://doi.org/10.1016/S1470-2045(17)30516-8.
4. Saridaki, Z., Souglakos, J., and Georgoulias, V. (2014). Prognostic and predictive significance of MSI in stages II/III colon cancer. World J. Gastroenterol. *20*, 6809–6814. https://doi.org/10.3748/wjg.v20.i22.6809.
5. Amodio, V., Mauri, G., Reilly, N.M., Sartore-Bianchi, A., Siena, S., Bardelli, A., and Germano, G. (2021). Mechanisms of immune escape and resistance to checkpoint inhibitor therapies in mismatch repair deficient metastatic colorectal cancers. Cancers *13*, 2638. https://doi.org/10.3390/cancers13112638.

6. Hause, R.J., Pritchard, C.C., Shendure, J., and Salipante, S.J. (2016). Classification and characterization of microsatellite instability across 18 cancer types. Nat. Med. *22*, 1342–1350. https://doi.org/10.1038/nm.4191.

7. Cortes-Ciriano, I., Lee, S., Park, W.Y., Kim, T.M., and Park, P.J. (2017). A molecular portrait of microsatellite instability across multiple cancers. Nat. Commun. *8*, 15180. https://doi.org/10.1038/ncomms15180.

8. Benson, A.B., Venook, A.P., Al-Hawary, M.M., Arain, M.A., Chen, Y.J., Ciombor, K.K., Cohen, S., Cooper, H.S., Deming, D., Farkas, L., et al. (2021). Colon cancer, Version 2.2021, NCCN clinical practice guidelines in Oncology. J. Natl. Compr. Canc. Netw. *19*, 329–359. https://doi.org/10.6004/jnccn.2021.0012.

9. Le, D.T., Uram, J.N., Wang, H., Bartlett, B.R., Kemberling, H., Eyring, A.D., Skora, A.D., Luber, B.S., Azad, N.S., Laheru, D., et al. (2015). PD-1 blockade in tumors with mismatch-repair deficiency. N. Engl. J. Med. *372*, 2509–2520. https://doi.org/10.1056/NEJMoa1500596.

10. Overman, M.J., Lonardi, S., Wong, K.Y.M., Lenz, H.J., Gelsomino, F., Aglietta, M., Morse, M.A., Van Cutsem, E., McDermott, R., Hill, A., et al. (2018). Durable clinical benefit with Nivolumab plus Ipilimumab in DNA mismatch repair-deficient/microsatellite instability-high metastatic colorectal cancer. J. Clin. Oncol. *36*, 773–779. https://doi.org/10.1200/JCO.2017.76.9901.

11. Rousseau, B., Foote, M.B., Maron, S.B., Diplas, B.H., Lu, S., Argilés, G., Cercek, A., and Diaz, L.A. (2021). The spectrum of benefit from checkpoint blockade in hypermutated tumors. N. Engl. J. Med. *384*, 1168–1170. https://doi.org/10.1056/NEJMc2031965.

12. Marabelle, A., Le, D.T., Ascierto, P.A., Di Giacomo, A.M., De Jesus-Acosta, A., Delord, J.P., Geva, R., Gottfried, M., Penel, N., Hansen, A.R., et al. (2020). Efficacy of pembrolizumab in patients with Noncolorectal high microsatellite instability/mismatch repair-deficient cancer: results from the phase II KEYNOTE-158 study. J. Clin. Oncol. *38*, 1–10. https://doi.org/10.1200/JCO.19.02105.

13. Shia, J., Ellis, N.A., and Klimstra, D.S. (2004). The utility of immunohistochemical detection of DNA mismatch repair gene proteins. Virchows Arch. *445*, 431–441. https://doi.org/10.1007/s00428-004-1090-5.

14. Kastrinos, F., and Syngal, S. (2012). Screening patients with colorectal cancer for Lynch syndrome: what are we waiting for? J. Clin. Oncol. *30*, 1024–1027. https://doi.org/10.1200/JCO.2011.40.7171.

15. Beamer, L.C., Grant, M.L., Espenschied, C.R., Blazer, K.R., Hampel, H.L., Weitzel, J.N., and MacDonald, D.J. (2012). Reflex immunohistochemistry and microsatellite instability testing of colorectal tumors for Lynch syndrome among US cancer programs and follow-up of abnormal results. J. Clin. Oncol. *30*, 1058–1063. https://doi.org/10.1200/JCO.2011.38.4719.

16. Luchini, C., Bibeau, F., Ligtenberg, M.J.L., Singh, N., Nottegar, A., Bosse, T., Miller, R., Riaz, N., Douillard, J.Y., Andre, F., and Scarpa, A. (2019). ESMO recommendations on microsatellite instability testing for immunotherapy in cancer, and its relationship with PD-1/PD-L1 expression and tumour mutational burden: a systematic review-based approach. Ann. Oncol. *30*, 1232–1243. https://doi.org/10.1093/annonc/mdz116.

17. McCarthy, A.J., Capo-Chichi, J.M., Spence, T., Grenier, S., Stockley, T., Kamel-Reid, S., Serra, S., Sabatini, P., and Chetty, R. (2019). Heterogenous loss of mismatch repair (MMR) protein expression: a challenge for immunohistochemical interpretation and microsatellite instability (MSI) evaluation. J. Pathol. Clin. Res. *5*, 115–129. https://doi.org/10.1002/cjp2.120.

18. Kim, S.T., Cristescu, R., Bass, A.J., Kim, K.M., Odegaard, J.I., Kim, K., Liu, X.Q., Sher, X., Jung, H., Lee, M., et al. (2018). Comprehensive molecular characterization of clinical responses to PD-1 inhibition in metastatic gastric cancer. Nat. Med. *24*, 1449–1458. https://doi.org/10.1038/s41591-018-0101-z.

19. Fusco, N., Lopez, G., Corti, C., Pesenti, C., Colapietro, P., Ercoli, G., Gaudioso, G., Faversani, A., Gambini, D., Michelotti, A., et al. (2018). Mismatch repair protein loss as a prognostic and predictive biomarker in breast cancers regardless of microsatellite instability. JNCI Cancer Spectr. *2*, pky056. https://doi.org/10.1093/jncics/pky056.

20. Loupakis, F., Maddalena, G., Depetris, I., Murgioni, S., Bergamo, F., Dei Tos, A.P., Rugge, M., Munari, G., Nguyen, A., Szeto, C., et al. (2019). Treatment with checkpoint inhibitors in a metastatic colorectal cancer patient with molecular and immunohistochemical heterogeneity in MSI/dMMR status. J. Immunother. Cancer *7*, 297. https://doi.org/10.1186/s40425-019-0788-5.

21. Watkins, J.C., Nucci, M.R., Ritterhouse, L.L., Howitt, B.E., and Sholl, L.M. (2016). Unusual mismatch repair immunohistochemical patterns in endometrial carcinoma. Am. J. Surg. Pathol. *40*, 909–916. https://doi.org/10.1097/PAS.0000000000000663.

22. Chapusot, C., Martin, L., Bouvier, A.M., Bonithon-Kopp, C., Ecarnot-Laubriet, A., Rageot, D., Ponnelle, T., Laurent Puig, P., Faivre, J., and Piard, F. (2002). Microsatellite instability and intratumoural heterogeneity in 100 right-sided sporadic colon carcinomas. Br. J. Cancer *87*, 400–404. https://doi.org/10.1038/sj.bjc.6600474.

23. Greenberg, A., Kariv, R., Solar, I., and Hershkovitz, D. (2020). Geographic heterogeneity for mismatch repair proteins is associated with defects in DNA repair. Isr. Med. Assoc. J. *22*, 32–36.

24. Tachon, G., Frouin, E., Karayan-Tapon, L., Auriault, M.L., Godet, J., Moulin, V., Wang, Q., and Tougeron, D. (2018). Heterogeneity of mismatch repair defect in colorectal cancer and its implications in clinical practice. Eur. J. Cancer *95*, 112–116. https://doi.org/10.1016/j.ejca.2018.01.087.

25. Joost, P., Veurink, N., Holck, S., Klarskov, L., Bojesen, A., Harbo, M., Baldetorp, B., Rambech, E., and Nilbert, M. (2014). Heterogenous mismatch-repair status in colorectal cancer. Diagn. Pathol. *9*, 126. https://doi.org/10.1186/1746-1596-9-126.

26. Crisafulli, G., Sartore-Bianchi, A., Lazzari, L., Pietrantonio, F., Amatu, A., Macagno, M., Barault, L., Cassingena, A., Bartolini, A., Luraghi, P., et al. (2022). Temozolomide treatment alters mismatch repair and boosts mutational burden in tumor and blood of colorectal cancer patients. Cancer Discov. *12*, 1656–1675. https://doi.org/10.1158/2159-8290.CD-21-1434.

27. Germano, G., Lamba, S., Rospo, G., Barault, L., Magrì, A., Maione, F., Russo, M., Crisafulli, G., Bartolini, A., Lerda, G., et al. (2017). Inactivation of DNA repair triggers neoantigen generation and impairs tumour growth. Nature *552*, 116–120. https://doi.org/10.1038/nature24673.

28. Michel, S., Benner, A., Tariverdian, M., Wentzensen, N., Hoefler, P., Pommerencke, T., Grabe, N., von Knebel Doeberitz, M., and Kloor, M. (2008). High density of FOXP3-positive T cells infiltrating colorectal cancers with microsatellite instability. Br. J. Cancer *99*, 1867–1873. https://doi.org/10.1038/sj.bjc.6604756.

29. Cahill, D.P., Levine, K.K., Betensky, R.A., Codd, P.J., Romany, C.A., Reavie, L.B., Batchelor, T.T., Futreal, P.A., Stratton, M.R., Curry, W.T., et al. (2007). Loss of the mismatch repair protein MSH6 in human glioblastomas is associated with tumor progression during temozolomide treatment. Clin. Cancer Res. *13*, 2038–2045. https://doi.org/10.1158/1078-0432.CCR-06-2149.

30. Yip, S., Miao, J., Cahill, D.P., Iafrate, A.J., Aldape, K., Nutt, C.L., and Louis, D.N. (2009). MSH6 mutations arise in glioblastomas during temozolomide therapy and mediate temozolomide resistance. Clin. Cancer Res. *15*, 4622–4629. https://doi.org/10.1158/1078-0432.CCR-08-3012.

31. Yan, T., Berry, S.E., Desai, A.B., and Kinsella, T.J. (2003). DNA mismatch repair (MMR) mediates 6-thioguanine genotoxicity by introducing single-strand breaks to signal a G2-M arrest in MMR-proficient RKO cells. Clin. Cancer Res. *9*, 2327–2334.

32. Chen, L., Yan, H.X., Liu, X.W., and Chen, W.X. (2020). Clinical efficacy and safety of 6-thioguanine in the treatment of childhood acute lymphoblastic leukemia: a protocol for systematic review and meta-analysis. Medicine (Baltim.) *99*, e20082. https://doi.org/10.1097/MD.0000000000020082.

33. Walbert, T., Gilbert, M.R., Groves, M.D., Puduvalli, V.K., Yung, W.K.A., Conrad, C.A., Bobustuc, G.C., Colman, H., Hsu, S.H., Bekele, B.N., et al. (2011). Combination of 6-thioguanine, capecitabine, and celecoxib with temozolomide or lomustine for recurrent high-grade glioma. J. Neuro Oncol. *102*, 273–280. https://doi.org/10.1007/s11060-010-0313-7.

34. André, T., Shiu, K.K., Kim, T.W., Jensen, B.V., Jensen, L.H., Punt, C., Smith, D., Garcia-Carbonero, R., Benavides, M., Gibbs, P., et al. (2020).

Pembrolizumab in microsatellite-instability-high advanced colorectal cancer. N. Engl. J. Med. *383*, 2207–2218. https://doi.org/10.1056/NEJMoa2017699.

35. Pietrantonio, F., Lobefaro, R., Antista, M., Lonardi, S., Raimondi, A., Morano, F., Mosconi, S., Rimassa, L., Murgioni, S., Sartore-Bianchi, A., et al. (2020). Capecitabine and temozolomide versus FOLFIRI in RAS-mutated, MGMT-methylated metastatic colorectal cancer. Clin. Cancer Res. *26*, 1017–1024. https://doi.org/10.1158/1078-0432.CCR-19-3024.
36. Konits, P.H., Egorin, M.J., Van Echo, D.A., Aisner, J., Andrews, P.A., May, M.E., Bachur, N.R., and Wiernik, P.H. (1982). Phase II evaluation and plasma pharmacokinetics of high-dose intravenous 6-thioguanine in patients with colorectal carcinoma. Cancer Chemother. Pharmacol. *8*, 199–203. https://doi.org/10.1007/BF00255484.
37. Pietrantonio, F., Perrone, F., de Braud, F., Castano, A., Maggi, C., Bossi, I., Gevorgyan, A., Biondani, P., Pacifici, M., Busico, A., et al. (2014). Activity of temozolomide in patients with advanced chemorefractory colorectal cancer and MGMT promoter methylation. Ann. Oncol. *25*, 404–408. https://doi.org/10.1093/annonc/mdt547.
38. Amatu, A., Barault, L., Moutinho, C., Cassingena, A., Bencardino, K., Ghezzi, S., Palmeri, L., Bonazzina, E., Tosi, F., Ricotta, R., et al. (2016). Tumor MGMT promoter hypermethylation changes over time limit temozolomide efficacy in a phase II trial for metastatic colorectal cancer. Ann. Oncol. *27*, 1062–1067. https://doi.org/10.1093/annonc/mdw071.
39. Evensen, N.A., Madhusoodhan, P.P., Meyer, J., Saliba, J., Chowdhury, A., Araten, D.J., Nersting, J., Bhatla, T., Vincent, T.L., Teachey, D., et al. (2018). MSH6 haploinsufficiency at relapse contributes to the development of thiopurine resistance in pediatric B-lymphoblastic leukemia. Haematologica *103*, 830–839. https://doi.org/10.3324/haematol.2017.176362.
40. Morano, F., Raimondi, A., Pagani, F., Lonardi, S., Salvatore, L., Cremolini, C., Murgioni, S., Randon, G., Palermo, F., Antonuzzo, L., et al. (2022). Temozolomide followed by combination with low-dose Ipilimumab and Nivolumab in patients with microsatellite-stable. J. Clin. Oncol. *40*, 1562–1573. https://doi.org/10.1200/JCO.21.02583.
41. Marmorino, F., Boccaccino, A., Germani, M.M., Falcone, A., and Cremolini, C. (2020). Immune checkpoint inhibitors in pMMR metastatic colorectal cancer: a tough challenge. Cancers *12*, 2317. https://doi.org/10.3390/cancers12082317.
42. Sanjana, N.E., Shalem, O., and Zhang, F. (2014). Improved vectors and genome-wide libraries for CRISPR screening. Nat. Methods *11*, 783–784. https://doi.org/10.1038/nmeth.3047.
43. Li, W., Xu, H., Xiao, T., Cong, L., Love, M.I., Zhang, F., Irizarry, R.A., Liu, J.S., Brown, M., and Liu, X.S. (2014). MAGeCK enables robust identification of essential genes from genome-scale CRISPR/Cas9 knockout screens. Genome Biol. *15*, 554. https://doi.org/10.1186/s13059-014-0554-4.
44. Dijkstra, K.K., Cattaneo, C.M., Weeber, F., Chalabi, M., van de Haar, J., Fanchi, L.F., Slagter, M., van der Velden, D.L., Kaing, S., Kelderman, S., et al. (2018). Generation of tumor-reactive T cells by Co-culture of peripheral blood lymphocytes and tumor organoids. Cell *174*, 1586–1598.e12. https://doi.org/10.1016/j.cell.2018.07.009.
45. Shalem, O., Sanjana, N.E., Hartenian, E., Shi, X., Scott, D.A., Mikkelson, T., Heckl, D., Ebert, B.L., Root, D.E., Doench, J.G., and Zhang, F. (2014). Genome-scale CRISPR-Cas9 knockout screening in human cells. Science *343*, 84–87. https://doi.org/10.1126/science.1247005.

STAR★METHODS

KEY RESOURCES TABLE

REAGENT or RESOURCE	SOURCE	IDENTIFIER
Antibodies		
In Vivo Mab Anti-Mouse CD8a	Bioxcell	Cat#BE0061; RRID: AB_1125541
In Vivo Mab Anti-Mouse γ/δTCR	Bioxcell	Cat#BE0070; RRID: AB_1107751
Recombinant antiMLH1 antibody	Abcam	Cat#Ab92312; RRID: AB_2049968
Anti β-actin (C4)	Santa Cruz Biotechnology	Cat#Sc-47778; RRID: AB_626632
PE-Cy7 Rat anti-mouse CD45 (30-F11)	BD biosciences	Cat#552848; RRID: AB_394489
BB700 Armenian Hamster anti-mouse CD3e (145-2C11)	BD biosciences	Cat#566494; RRID: AB_2744393
BV786 Rat anti-mouse CD4 (RM4-5)	BD biosciences	Cat#563727; RRID: AB_2728707
APC anti-mouse CD8a (53-6.7)	BD biosciences	Cat#553035 RRID: AB_398527
BB515 Rat anti-CD11b (M1/70)	BD biosciences	Cat#564454; RRID: AB_2665392
APCR-700 Rat anti-mouse CD25 (PC61)	BD biosciences	Cat#565134; RRID: AB_2744344
BV421 Hamster anti-mouse γδ T cell receptor (GL3)	BD bioscences	Cat#562892 RRID: AB_2737871
PE-CF594 Rat anti-mouse FOXP3 (MF23)	BD bioscences	Cat#562466 RRID: AB_11151905
BV480 hamster anti-mouse CD49b (HMα2)	BD bioscences	Cat#746355; RRID:AB_2743674
BV605 Rat anti-mouse CD19 (1D3)	BD bioscences	Cat#563148 RRID:AB_2732057
BD PharmingenTM Purified Rat Anti-Mouse CD16/CD32 (Mouse BD Fc BlockTM)	BD bioscences	Cat#553141; RRID: AB_394656
APC Anti-mouse F4/80 Antibody	Biolegend	Cat#123116 RRID: AB_893481
Hamster anti-mouse CD28	eBioscience	16-0281-85 RRID: AB_468921
PE Rat Anti-Mouse IFN-γ	BD Biosciences	Cat#562020 RRID: AB_395376
PerCP-Cy™5.5 Rat Anti-Mouse CD3 Molecular Complex	BD Biosciences	Cat#560527 RRID: AB_1727463
FITC Rat Anti-Mouse CD4	BD Biosciences	Cat#557307 RRID: AB_395013
Bacterial and virus strains		
Endura Chemically Competent Cells	Lucigen	Cat#60241-1
Chemicals, peptides, and recombinant proteins		
6-Thioguanine	Selleckchem	Cat#S1774
Temozolomide	Carbosynth	Cat#FT28027
Ficoll Paque Plus	Cytiva	Cat#17-1440-02
Recombinant Mouse IL-2 Protein	R&D system	Cat#402-ML-100
Golgi-Plug	BD Biosciences	Cat#555029
Golgi-Stop	BD Biosciences	Cat#554724

(*Continued on next page*)

Continued

REAGENT or RESOURCE	SOURCE	IDENTIFIER
Lipofectamine 2000	Thermo Fisher Scientific	Cat#11668027
Lipofectamine 3000	Thermo Fisher Scientific	Cat#L3000008
Critical commercial assays		
ReliaPrepTM gDNA Tissue Miniprep System	Promega	Cat#A2051
Cytofix/Cytoperm kit	BD Biosciences	Cat#554714
Live/dead fixable near-IR dead cell stain kit	Invitrogen	Cat#L10119
MiSeq® Reagent Kit v3 (150 cycle)	Illumina	Cat#MS-102-3001
ddPCR Supermix for Probes (No dUTP)	Biorad	Cat#1863025
High sensitivity DNA kit	Agilent	Cat#5067-4626
Deposited data		
Raw sequencing data related to Figure S4	European Nucleotide Archive (ENA) at EMBL-EBI (https://www.ebi.ac.uk/ena/browser/view/PRJEB56611)	ENA: PRJEB56611
Experimental models: Cell lines		
CT26	ATCC	Cat# CRL-2638, RRID:CVCL_7256
CT26 *Mlh1*$^{+/+}$ clone	This paper	N/A
CT26 *Mlh1*$^{-/-}$ clone	This paper	N/A
Experimental models: Organisms/strains		
Balb/C mouse	Charles River	Cat# 028
NODSCID mouse	Charles River	Cat# 634
Oligonucleotides		
ddPCR™ NHEJ Genome Edit Detection Assay (detection mut.mMlh1)	Biorad	Cat#dNHS185016514 https://www.bio-rad.com/digital-assays/assay-detail/dNHS185016514
ddPCR™ Mutation Assay (detection mut.mKras)	Biorad	Cat#dMDS202760100 https://www.bio-rad.com/digital-assays/assay-detail/dMDS202760100
Recombinant DNA		
LentiCRISPR-v2	Addgene[42]	Cat#52961 RRID:Addgene_52961
pLV[gRNA]-Puro-U6>gRNA	VectorBuilder	Cat#Lib180919-1186gax
pMD2.G	Addgene	Cat#12259 RRID:Addgene_12259
psPAX2	Addgene	Cat#12260 RRID:Addgene_12260
Software and algorithms		
GraphPad Prism	GraphPad	https://www.graphpad.com/scientific-software/prism/
FlowJo	BD	https://www.flowjo.com/solutions/flowjo/downloads
QuantaSoftTM Analysis Pro Software (Bio-Rad)	Biorad	N/A
MAGeCK	Wei Li, Han Xu, et al.[43]	https://github.com/liulab-dfci/MAGeCK
Other		
APC-H7 LIVE/DEAD Fixable Viability Stain 780	BD biosciences	Cat#565388 RRID: AB_2869673
BD PharmingenTM Transcription Factor Buffer Set	BD Bioscences	Cat#562574; RRID: AB_2869424
BD HorizonTM Brilliant Stain Buffer	BD Bioscences	Cat#563794

RESOURCE AVAILABILITY

Lead contact

Further information and requests for resources and reagents should be directed to and will be fulfilled by the lead contact Prof. Alberto Bardelli (alberto.bardelli@unito.it).

Materials availability

Mouse cell lines generated for this study will be shared upon request under an MTA handled by the University of Torino.

Data and code availability

Standardized datatype used for the generation of Figure S4 have been deposited in the European Nucleotide Archive (ENA) at EMBL-EBI and are publicly available as of the date of publication (https://www.ebi.ac.uk/ena/browser/view/PRJEB56611). Accession number (ENA: PRJEB56611) is listed also in the key resources table.

All the other data reported in this paper will be shared by the lead contact upon request.

This paper does not report original code.

Any additional information required to reanalyse the data reported in this paper is available from the lead contact upon request.

EXPERIMENTAL MODEL AND SUBJECT DETAILS

Mouse cell line

CT26 is a murine undifferentiated colon carcinoma cell line obtained from a BALB C background. CT26 were purchased from ATCC and were cultured in RPMI 1640 10% FBS, 1% glutamine and 1% penicillin/streptomycin. Cell line was propagated three times a week to ensure the best fitness in the plate. Prior the execution of the experiments reported in this manuscript, parental cell line was injected in the syngeneic background and the resulting tumor was exploited to re-establish *in vitro* a new cell culture. This procedure ensures that the models used are tumorigenic and will be not edited from the immune system of the syngeneic model in the following application. Cell were tested for mycoplasma detection regularly.

Animal studies

All animal procedures were approved by the Ethical Commission of the University of Turin and by the Italian Ministry of Health. All *in vivo* experiments were executed according to institutional guidelines and international law and policies and following methods previously described.[27] We used five-to ten-weeks old female BALB C (immunocompetent mice, Cat#028) and NOD SCID mice (immunocompromised mice, Cat#634) purchased from Charles River (Calco, Como Italy). Each experiment was performed using at least five mice per group. The number of mice for each experiment is reported in figure legends. For subcutaneous injection (CT26), mice were shaved, and 5 x 10^5 cells resuspended in 100 μL of PBS were injected on the right flank. For the abscopal experiment (Figure 3), 2,5 x 10^5 cells were simultaneously injected in 100 μL PBS in both flanks. For the seeding experiment reported in Figure 1, the number of the cells injected is reported in the legend and in the figure.

Tumor size was measured twice a week and volume was calculated using the formula: $V = (d^2 \times D)/2$ (d = minor tumor axis; D = major tumor axis) and reported as tumor volume (mm^3, mean ± SEM of individual tumor volume). Mice were maintained in individually ventilated cages containing refinement instruments. Animal welfare was checked by veterinary personnel during all the experiments. Mice were daily monitored for social behaviors, compromised motility and sign of distress. As soon as mice fitness was impaired or mice displayed sign of pain, animals were sacrificed in accordance with humane endpoint. For the experiments reported in this work, sample size was not pre-determined using statistical methods. Selection and exclusion criteria of mice from the analyses, when applied, have been indicate in figure legends. Animals were not previously involved in other experimental procedures. The investigators did not operate in blind.

METHOD DETAILS

Gene editing

The knock-out of the *Mlh1* gene in mouse cells was generated using the genome editing one vector system (lentiCRISPR-v2) (Addgene #52961)[42] as previously reported.[27] To reduce off-target effects, CRISPR tool http://crispr.mit.edu was deployed to design sgRNAs. For these experiments, we needed transient expression of CRISPR-Cas9 system, consequently we transfected cells with lentiCRISPR-v2 vector plasmid as previously reported.[27] Transfection was performed using Opti-MEM (Invitrogen) and Lipofectamine 3000 (Life Technologies). After 2 days, cells were treated with puromycin (Sigma Aldrich) for 5 days and then single cell dilution was performed in 96-well plates for each guide. The knock-out of *Mlh1* was evaluated by western blot.

Mouse treatments

6TG was purchased from Selleckchem and was dissolved in a stock solution of 15 mg/mL in DMSO. *In vivo* 6TG treatment (3 mg/kg) was started 5 days after injection and was administered intraperitoneally daily for 5 treatments in total. 6TG working solution was prepared diluting stock solution in PBS daily and DMSO treatment was used as control arm. Mice were randomized before starting treatment according to the tumor volumes.

In Vivo Mab Anti-Mouse CD8a (Bioxcell, BE0061) was administered following the schedule: 400 μg day 0, 200 μg day 2 post tumor injection and then every 3 days. *In vivo* Mab Anti-Mouse TCR γ/δ (BE0070) cells antibody was administrated following the schedule: 400μg day −2, −1, +3 + 6 post tumor injection and then every 7 days.

Western Blot analyses

For western blot assays, cells were cultured in media containing 10% FBS. Proteins were extracted by lysing cell pellets in SDS buffer (50 mM Tris-HCl [pH 7.5], 150 mM NaCl, and 1% SDS). Samples were boiled at 95°C for 10 min and sonicated for 15–30 s depending on the dimension of the pellet. Eventual residual debris were pelleted by centrifugation and 5 μL of supernatant were used to quantify the protein content. Quantification phase was performed using BCA Protein Assay Reagent Kit (Thermo Scientific). Detection phase was conducted with the enhanced chemiluminescence system (GE Healthcare) and peroxidase-conjugated secondary antibodies (Amersham). The primary antibodies used for this assay were: anti mMLH1 (epr3894 from Abcam), anti Actin (C4) from Santa Cruz Biotechnology.

Genomic DNA extraction

Genomic DNA was extracted from SNP Frozen preserved cell pellets and SNP Frozen tumor fragments using Maxwell Instrument (Promega) or ReliaPrep gDNA Tissue Miniprep System (Promega). To achieve a realistic image about the composition of tumor content in terms of *Mlh1*$^{-/-}$ and *Mlh1*$^{+/+}$ cells, we extracted gDNA form the entire mass, dividing each tumor in several small pieces and then pooling together the extracted material.

Droplet digital PCR detection

Genomic DNA was amplified using ddPCR Supermix for Probes (No dUTP) (Bio-Rad) with the murine *Kras* G12D custom assay (https://www.bio-rad.com/digital-assays/assay-detail/dMDS202760100) and a ddPCR Non-Homologous End-Joining (NHEJ) Genome Edit Detection assay (BioRad) for murine *Mlh1* (https://www.bio-rad.com/digital-assays/assay-detail/dNHS185016514). ddPCR was then performed according to manufacturer's protocol, and the results were reported as the percentage or fractional abundance of mutant DNA alleles to total (mutant plus wild-type) DNA alleles. 5–10 μL of DNA template was added to 10 μL of ddPCR Supermix for Probes (Bio-Rad) and 2 μL of the primer and probe mixture. Droplets were generated using the Automated Droplet Generator (Auto-DG, Bio-Rad) where the reaction mix was added together with Droplet Generation Oil for Probes (Bio-Rad). Droplets were then transferred to a 96 well plate and then thermal cycled with different program based on the assay and according to the manufacturer's protocol. Droplets were analyzed with the QX200 Droplet Reader (Bio-Rad) for fluorescent measurement of FAM and HEX probes. Gating was performed based on positive and negative controls, and mutant populations were identified. The ddPCR data were analyzed with QuantaSoft Analysis Pro Software (Bio-Rad) to obtain fractional abundance of the mutated DNA alleles in the wild-type or normal background. The quantification of the target molecule was presented as number of total copies (mutant plus WT/edited plus unedited) per sample in each reaction. Fractional abundance (F.A.) is calculated as follows: F.A. % = (Nmut/(Nmut + Nwt)) × 100) for KRAS G12D assay (where Nmut is the number of mutant events and Nwt is the number of WT events per reaction) or F.A. % = NHEJ edited alleles/(wild-type + NHEJ edited alleles), in other words, edited alleles/total alleles (edited + unedited). To precisely determine the *Mlh1* status of each tumor, two or three independent sampling were performed and analyzed.

In vitro enrichment assay

CT26 *Mlh1*$^{+/+}$ and *Mlh1*$^{-/-}$ mixed populations were plated in 6 multiwell plates (100,000 cells/well). After 24 h cells were treated *in vitro* with DMSO, 6TG 1 μM or TMZ 200uM. At two different time points, day 4 and day 7-8, cell gDNA was extracted. *Mlh1*$^{-/-}$ cell percentage was evaluated throughout droplet digital PCR assays as previously reported. For the second timepoint, all cells were split (1:10) on day 4. Three technical and biological replicates were performed for each condition.

Immunophenotyping

Whole tumors were explanted, stored at 4°C for 24 h in MACS tissue storage solution (Miltenyi) and dissociated with Tumor dissociation Kit from Miltenyi biotechnology. After a first step of mechanical smashing with Gentle Macs Dissociation Kit, tumors were enzymatically digested for 30 min at 37°C as indicated in the protocol of dissociation kit. Flow cytometry analyses were performed using Symphony (BD Biosciences). Immune staining was performed using the following antibodies purchased by BD Biosciences: PE-Cy7 Rat anti-mouse CD45 (30-F11), BB700 anti-mouse CD3e (145-2C11), BV786 Rat anti-mouse CD4 (RM4-5), APC anti-mouse CD8a (53-6.7), BB515 Rat anti-human/mouse CD11b (M1/70), APCR-700 Rat anti-mouse CD25 (PC61), BV421 Hamster anti-mouse γδ T-Cell Receptor(GL3), PE-CF594 anti mouse FOXP3 (MF23), BV480 hamster anti-mouse CD49b (HMα2), BV605 Rat anti-mouse CD19 (1D3), APC-H7 LIVE/DEAD Fixable Viability Stain 780. APC anti-mouse F4/80 was purchased by Biolegend. BD Pharmingen Purified Rat Anti-Mouse CD16/CD32 (Mouse BD Fc Block), BD Pharmingen Transcription Factor Buffer Set, BD Horizon Brilliant Stain Buffer were used during the staining procedure as indicated in the protocols. Analyses were performed using FlowJo software.

In vitro reactivity

CT26 cell populations (CT26 100% *Mlh1*$^{+/+}$ and 50% *Mlh1*$^{-/-}$ 50% *Mlh1*$^{+/+}$) were injected in immunocompetent BALB C mice. On day 13, mice were sacrificed and blood was harvested. Blood collected from three mice was pooled for each experimental group. PBMC were isolated by Ficoll density gradient separation (Lympholyte H) and were let to rest overnight in culturing medium

(RPMI + mouse-recombinant Interleukin-2 50U/ml). The day after, 1 x 10^5 PBMC were seeded in anti-CD28-coated plates with CT26 *Mlh1*$^{+/+}$ or CT26 *Mlh1*$^{-/-}$ *cells* separately (1:1 PBMC: tumor cells ratio), and cocultured for 5 h. Golgi-Plug (1:1000, BD) and Golgi-Stop (1:1500, BD) were added after 1h and coculture continued for an additional 4 h. Cells were washed twice in FACS buffer and stained with the following surface antibodies mixes for 30 min at 4C: near-IR viability Dye, anti-CD3-PerCP-Cy5.5, anti-γδTCR-BV421, anti-CD4-FITC, anti-CD8-APC. Cells were washed twice in FACS buffer, fixed and stained for intracellular IFNγ (anti-IFNγ-PE) using Cytofix/Cytoperm kit (BD), according to manufacturer's instructions. PBMC cultured without tumor stimulation served as negative control. The percentage of IFNγ$^+$ cells was calculated above the background (the background value was subtracted). Only immune population in which at least two biological replicates were above the threshold of 1% of IFNγ$^+$ cells were considered reactive as previously reported.[44]

DNA damage response (DDR) library design and lentiviral production

We synthetized a custom library, targeting 488 DDR genes (constructed by VectorBuilder, ID: Lib180919-1186gax) (Table S1). For each gene 6 guides (sgRNA) were selected and we included 100 not target guides as control. The guides have been synthesized and cloned in pLV[gRNA]-Puro-U6>gRNA -based Gene Knockout sgRNA, containing puromycin cassette as selection.

To generate lentivirus, the transfer plasmids were co-transfected with packaging plasmids pMD2.G (Addgene #12259) and psPAX2 (Addgene #12260) as described previously.[45] HEK293T cells 80% confluent was transfected in OptiMEM (Life Technologies) using Lipofectamine 2000 (Life Technologies). After 52 h, the supernatant was filtered and stored. Lentiviruses were tittered in a functional assay by measuring puromycin resistance after transduction. Optimal infection conditions were determined for each cell line to achieve 20–30% infection efficiency, corresponding to a MOI of ~0.2–0.3. Screening-scale infections were performed with the predetermined volume of virus in the same format as the viral titration described above and pooled 12 h post-centrifugation. Based on library size, infections were performed with enough cells to achieve a representation of ~500 cells per sgRNA in the library.

Cas9-expressing clone were infected with enough cells to achieve a representation of ~500 cells per sgRNA in the library at a MOI of 0.3. Cells were selected with puromycin for 5–6 days following infection to remove uninfected cells.

6TG (1μM, Selleckchem) or TMZ (100 μM, Carbosynth) was added to puromycin-selected cells 7 days post-infection. Surviving cells were harvested after 14 days of treatment. The fold-change of each sgRNA was determined relative to the starting T0 pool for each biological replicate.

Library sequencing and bioinformatic analysis of NGS data

Genomic DNA was isolated from cell pellets using the QIAAmp DNA Blood Midi Kit - QIAGEN. The sgRNA spanning region was amplified from purified genomic with primers to add Illumina adapters and indices. The PCR product was purified and size selected on gel and the correct fragment size was confirmed with a High Sensitivity Bioanalyzer DNA Kit (Agilent). Sequencing was performed on an Illumina Miseq system.

Sequence analysis was performed on all samples in order to quantify each different sgRNA. Negative and positive selection analysis was performed using the "test" function from MAGeCK tool[43] with default parameters and the results was finally filtered to have a statistically significant false discovery rate (FDR)

QUANTIFICATION AND STATISTICAL ANALYSIS

The number of biological replicates and sample size for *in vivo* experiments were adjusted according to requirements from the Italian Ministry of Health. For *in vitro* experiments, statistical differences between each experimental group and the control group were calculated using One Way ANOVA(multiple comparisons) and two-Way ANOVA (multiple comparisons). For *in vivo* experiments, statistical significance for tumor growth was evaluated using non-parametric test (p values were adjusted with Mann-Whitney correction). Statistical parameters are reported in figure legends. Graphpad Prism was used to perform statistical analyses.